Submitted on Aug. 10th, 2017

JOURNAL OF THE ATMOSPHERIC SCIENCES

Statistical state dynamics of weak jets in barotropic beta-plane turbulence

NIKOLAOS A. BAKAS

Laboratory of Meteorology and Climatology, Department of Physics, University of Ioannina, Ioannina, Greece

NAVID C. CONSTANTINOU*

Scripps Institution of Oceanography, University of California San Diego, La Jolla, California, USA

PETROS J. IOANNOU

Department of Physics, National and Kapodistrian University of Athens, Athens, Greece

ABSTRACT

Using the statistical state dynamics (SSD) framework with a closure at second order, it has been demonstrated that in barotropic flows zonal jets emerge out of homogeneous turbulence through an instability of the homogeneous turbulent state. This instability occurs as the turbulence intensity increases. Furthermore, it was shown that for small supercriticality, i.e. for turbulence intensity just above the critical value for forming jets, the jet-forming instability follows Ginzburg–Landau (G–L) dynamics. In this work, the SSD framework is used to study the processes by which the jet-forming instability is halted by nonlinearity allowing the jets to equilibrate at finite amplitude. First, the predictions of the G–L dynamics are compared with those of the SSD dynamics closed at second order. It is demonstrated that the G–L dynamics accurately captures the qualitative behavior of the jet evolution. The nonlinear term of the G–L dynamics that halts the instability is decomposed into three different physical processes. Their relative importance in the equilibration process is then studied and the types of eddies that contribute positively in each process are identified. The main process that determines the amplitude of the zonal jets at small supercriticality turns out to be the requirement that as jets grow the increase of mean flow energy is counter-balanced by a decrease in the energy of the eddy field.

1. Introduction

Robust eddy-driven zonal jets are ubiquitous in planetary atmospheres (Ingersoll 1990; Ingersoll et al. 2004; Vasavada and Showman 2005). Laboratory experiments, theoretical studies and numerical simulations have shown that small-scale turbulence self-organizes into these large scale coherent structures and supports the jets against eddy mixing (Starr 1968; Huang and Robinson 1998; Read et al. 2007; Salyk et al. 2006). One of the simplest models, which is a testbed for theories regarding turbulence self-organization, is forced–dissipative barotropic turbulence on a beta-plane. It was first theoretically predicted that zonal jets in barotropic beta-plane turbulence spontaneously emerge out of a background of homogeneous turbulence through a bifurcation that occurs as the bottom drag or as the turbulence intensity vary (Farrell and Ioannou 2007; Srinivasan and Young 2012). Jet emergence through a bifurcation was then confirmed by comparing these predictions to direct numerical simulations (Constantinou et al. 2014a). Beyond the bifurcation point the jets grow in energy and equilibrate at a finite amplitude that depends on the planetary vorticity gradient, β, on the bottom drag and on the turbulence intensity and the length scale of the forcing.

An advantageous framework for addressing the jet-forming instability, as well as the resulting statistical equilibria of the finite amplitude jets that result from the jet-forming instability, is the study of the Statistical State Dynamics (SSD) of the turbulent flow. SSD is the dynamics that governs the statistics of the flow fields. However, evolving the unclosed hierarchy of the flow statistics is intractable; a turbulence closure is needed. Unlike the usual paradigm of homogeneous isotropic turbulence theories, when strong coherent flows coexist with the incoherent turbulent field the SSD of the turbulent flow is accurately captured by a second-order closure (Srinivasan and Young 2012; Tobias and Marston 2013; Constantinou et al. 2014a; Bakas and Ioannou 2014; Constantinou et al. 2014b; Thomas et al. 2014, 2015; Ait-Chaalal et al. 2016; Marston et al. 2016; Farrell et al. 2016). The reason why second-order closure is so successful when coherent mean flows are present, is that the dynamics is then dominated

* *Corresponding author address:* Navid Constantinou, Scripps Institution of Oceanography, University of California San Diego, 9500 Gilman Dr. #0213, La Jolla, CA 90293-0213, USA.
E-mail: navid@ucsd.edu

by the interaction of turbulence with the coherent flow; and this eddy–mean flow interaction is accurately captured at second-order.

Spontaneous jet formation was shown to occur as an instability of the SSD closed at second-order (Farrell and Ioannou 2003, 2007). This jet-forming instability is referred to as an "S3T instability" (S3T is the acronym of "stochastic structural stability theory" which is such a second-order closure of the SSD (Farrell and Ioannou 2003)) or as "zonostrophic instability" (Srinivasan and Young 2012). The instability arises from the interaction of the coherent mean flow, i.e. the jets, with the incoherent turbulence: up-gradient vorticity fluxes can transfer momentum from the incoherent turbulent eddy field to the mean flow forming jets. Bakas and Ioannou (2013b) and Bakas et al. (2015) studied in detail the eddy–mean flow dynamics underlying the instability in various parameter regimes: for example, as we vary the bottom drag, β, and the forcing length-scale. Bakas and Ioannou (2013b) and Bakas et al. (2015) determined which of the incoherent eddies induce up-gradient momentum fluxes and drive the instability, and which of the incoherent eddies induce down-gradient momentum fluxes drawing momentum from the mean flow and thus hinder jet formation. They also showed that the induced fluxes can be interpreted as resulting from shearing of wave-packets by the infinitesimal jet and discussed how in this regime in which the eddies are dissipated before they are sheared over by the weak jet, the resulting fluxes can be up-gradient.

The jet-forming instability has also another very interesting characterization. Parker and Krommes (2013), noted that the S3T jet-forming instability can be embedded in the theory of pattern formation (Hoyle 2006; Cross and Greenside 2009) and applied the tools and methods of pattern formation theory to study jet formation (Parker and Krommes 2013, 2014). Furthermore, Parker and Krommes (2014) demonstrated that at small supercriticality, that is when the turbulence intensity is just above the critical point predicted by S3T theory for jet formation, the nonlinear evolution of the zonal jets follow Ginzburg–Landau dynamics.

While the jet-forming instability was extensively studied, we lack a comprehensive understanding of the equilibration of the instability and the eddy–mean flow dynamics involved in supporting the finite amplitude jets. After the primary S3T jet-forming instability the jets that emerge undergo a series of transformations in structure before they settle to an equilibrated structure. S3T predicts that the equilibrated jet must be hydrodynamically stable, approaching neutrality under strong driving (Farrell and Ioannou 2007). For this reason the equilibrated jets assume the familiar structure with pointed eastward jets and parabolic westward jets with an amplitude scaling with the Rhines scale. Furthermore, the dynamical system of the second-order SSD can readily produce multiple equilibria consisting of flows with a different number of jets (Farrell and Ioannou 2007; Parker and Krommes 2013); and these multiple equilibria states were confirmed to exist in direct numerical simulations (Constantinou et al. 2014a). Transitions between the various jet attractors occur through secondary instabilities of the finite amplitude jets. These secondary instabilities, however, are not hydrodynamic instabilities of the jet itself, but they are S3T instabilities, that is instabilities that arise from the coupling between the jets and the turbulence and have analytic expression only in the SSD (Farrell and Ioannou 2003, 2007; Constantinou et al. 2014a; Parker 2014; Constantinou 2015).

In this work, we undertake the task of investigating the equilibration of the jet-forming instabilities as well as the secondary instabilities that occur. We revisit the small-supercriticality regime of Parker and Krommes (2014). We test the validity of the G–L approximation of the SSD through a comparison with fully nonlinear simulation of the SSD closed at second order (section 5). The impressive qualitative agreement allows us to probe the dynamics of the equilibration of the jet-forming instability through studying the G–L dynamics. We use methods similar to the ones developed by Bakas and Ioannou (2013b) and Bakas et al. (2015) to understand the eddy–mean flow dynamics involved in: *(i)* the equilibration of the jet-forming instability, *(ii)* the support of the jets at finite amplitude (section 6), and *(iii)* the secondary instabilities that the finite amplitude equilibrium jets are susceptible to (section 7).

2. Statistical dynamics of barotropic β-plane turbulence in the S3T approximation

Consider a non-divergent flow $\boldsymbol{u} = (u, v)$ on a β-plane with coordinates $\boldsymbol{x} = (x, y)$; x is the zonal direction and y the meridional direction. The flow is in an unbounded domain, unless otherwise indicated. The flow is derived from a streamfunction $\psi(\boldsymbol{x}, t)$ via $(u, v) = (-\partial_y \psi, \partial_x \psi)$. The relative vorticity of the flow is $\zeta \stackrel{\text{def}}{=} \partial_x v - \partial_y u = \Delta\psi$, with $\Delta \stackrel{\text{def}}{=} \partial_x^2 + \partial_y^2$ the Laplacian. With stochastic excitation and linear dissipation the relative vorticity evolves according to:

$$(\partial_t + \boldsymbol{u} \cdot \boldsymbol{\nabla})(\zeta + \beta y) = -r\zeta + \sqrt{\varepsilon}\xi \ . \tag{1}$$

Linear dissipation at the rate r parametrizes Ekman drag at the planetary surface. Turbulence is supported by the random stirring $\xi(\boldsymbol{x}, t)$ that injects energy in the flow at rate ε. This random stirring models vorticity sources from convection and/or baroclinic growth processes that are absent in barotropic dynamics. The random process ξ is assumed *(i)* to have zero mean, *(ii)* to be spatially and temporally statistically homogeneous, and *(iii)* to be temporally

delta-correlated but spatially correlated. Thus it satisfies:

$$\langle \xi(\boldsymbol{x},t)\rangle = 0 \quad \text{and} \tag{2a}$$

$$\langle \xi(\boldsymbol{x}_a,t_1)\xi(\boldsymbol{x}_b,t_2)\rangle = Q(\boldsymbol{x}_a-\boldsymbol{x}_b)\,\delta(t_1-t_2)\,, \tag{2b}$$

with $Q(\boldsymbol{x}_a-\boldsymbol{x}_b)$ the homogeneous spatial covariance of the forcing. Angle brackets denote ensemble averaging over realizations of the forcing. The forcing covariance is constructed by specifying a non-negative spectral power function $\hat{Q}(\boldsymbol{k})$ as:

$$Q(\boldsymbol{x}_a-\boldsymbol{x}_b) = \int \frac{\mathrm{d}^2\boldsymbol{k}}{(2\pi)^2}\,\hat{Q}(\boldsymbol{k})\,\mathrm{e}^{\mathrm{i}\boldsymbol{k}\cdot(\boldsymbol{x}_a-\boldsymbol{x}_b)}\,. \tag{3}$$

In this work, we consider forcing with spectrum:

$$\hat{Q}(\boldsymbol{k}) = 4\pi k_f\,\delta(k-k_f)\,[1+\gamma\cos(2\vartheta)]\,, \tag{4}$$

where $k \overset{\text{def}}{=} |\boldsymbol{k}|$, $\vartheta \overset{\text{def}}{=} \arctan(k_y/k_x)$, and $|\gamma|\leq 1$, so that $\hat{Q}(\boldsymbol{k}) \geq 0$. The forcing spectrum (4) excites only waves with total wavenumber k_f. The parameter γ determines the degree of anisotropy of the forcing (Srinivasan and Young 2014; Bakas et al. 2015). Here, we consider the case with $\gamma = 0$ that produces isotropic forcing, and the case with $\gamma = 1$ that produces a non-isotropic forcing favoring structures with smaller $|k_y|$, as if the vorticity injection was due to baroclinic growth processes. The forcing spectrum is normalized so that the total energy injection is unity, i.e. $\hat{Q}$ satisfies:

$$\int \frac{\mathrm{d}^2\boldsymbol{k}}{(2\pi)^2}\,\frac{\hat{Q}(\boldsymbol{k})}{2k^2} = 1\,. \tag{5}$$

Because $\xi(\boldsymbol{x},t)$ has been assumed temporally delta-correlated, the rate of energy injection in (1) by the stochastic excitation is independent of the state of the system and equal to ε.

Equation (1) is non-dimensionalized using the forcing length scale k_f^{-1} and the dissipation time scale r^{-1}. The non-dimensional variables are: $\zeta_* = \zeta/r$, $\boldsymbol{u}_* = \boldsymbol{u}/(k_f^{-1}r)$, $\xi_* = \xi/(k_f\sqrt{r})$, $\varepsilon_* = \varepsilon/(k_f^{-2}r^3)$, $\beta_* = \beta/(k_f r)$ and $r_* = 1$. Asterisks denote non-dimensional units. From here after we consider (1) to be non-dimensional with the asterisks dropped and with $r = 1$. The non-dimensional form of $\hat{Q}$ in (4) is obtained by setting $k_f = 1$.

The statistical state dynamics (SSD) of (1) in the S3T/CE2 second-order closure comprise the dynamics of the first cumulant of the vorticity field $\bar{\zeta}(\boldsymbol{x},t)$, and of the second cumulant $C(\boldsymbol{x}_a,\boldsymbol{x}_b,t) \overset{\text{def}}{=} \overline{\zeta'(\boldsymbol{x}_a,t)\zeta'(\boldsymbol{x}_b,t)}$, with $\zeta'(\boldsymbol{x},t) \overset{\text{def}}{=} \zeta(\boldsymbol{x},t) - \bar{\zeta}(\boldsymbol{x},t)$. The overbar here denotes any proper averaging operator (Monin and Yaglom 1973; Ait-Chaalal et al. 2016) that identifies the coherent motions of the flow and, additionally, satisfies the ergodic property that the average of any quantity is equal to an ensemble average over realizations of ξ, i.e. $\overline{(\cdot)} = \langle(\cdot)\rangle$. If the coherent component of the turbulence is zonal jets, then a zonal average is the appropriate averaging operator. If the coherent component of the flow includes planetary-scale waves embedded in a zonal flow, then we need to use as an averaging operator a Reynolds average over an intermediate temporal or spatial scale that produces the required temporal or spatial coarse-grained/fine-grained flow separation to satisfy the Reynolds properties of averages (Ait-Chaalal et al. 2016; Constantinou et al. 2016; Marston et al. 2016). In this study we investigate the equilibration of zonal jets and, thus, we consider the S3T dynamics with a zonal average.

The S3T equations governing the first and second cumulant of the flow are:

$$\partial_t \bar{u} = \mathscr{R}(C) - \bar{u}\,, \tag{6a}$$

$$\partial_t C = -\mathscr{L}C + \mathscr{N}(\bar{u},C) + \varepsilon\,Q\,, \tag{6b}$$

where $\bar{u}(y,t)$ is the zonal-mean zonal velocity of the jet ($\bar{\zeta} = -\partial_y\bar{u}$), $C(x_a-x_b,y_a,y_b,t)$ is the eddy vorticity covariance, which is homogeneous in x,

$$\mathscr{L} \overset{\text{def}}{=} \beta\left(\partial_{x_a}\Delta_a^{-1} + \partial_{x_b}\Delta_b^{-1}\right) + 2\,, \tag{7}$$

is the operator governing the linear eddy dynamics, and

$$\mathscr{N}(\bar{u},C) \overset{\text{def}}{=} \left[-\bar{u}_a\,\partial_{x_a} + (\partial_{y_a}^2\bar{u}_a)\,\partial_{x_a}\Delta_a^{-1} - \bar{u}_b\,\partial_{x_b} + (\partial_{y_b}^2\bar{u}_b)\,\partial_{x_b}\Delta_b^{-1}\right] C\,, \tag{8}$$

is the nonlinear operator governing the interaction between the eddies and the instantaneous mean flow $\bar{u}(y,t)$. Subscripts a or b in operators acting on C indicate the point of evaluation and the specific variable the operator is acting on. The mean flow $\bar{u}$ is driven by the ensemble mean eddy vorticity flux[1]:

$$\mathscr{R}(C) \overset{\text{def}}{=} \frac{1}{2}\left[\left(\partial_{x_a}\Delta_a^{-1} + \partial_{x_b}\Delta_b^{-1}\right)C\right]_{a=b}\,, \tag{9}$$

in which subscript $a = b$ indicates that the function of $\boldsymbol{x}_a$ and $\boldsymbol{x}_b$, e.g., inside the square brackets in the r.h.s. of (9), is transformed into a function of a single variable by setting $\boldsymbol{x}_a = \boldsymbol{x}_b = \boldsymbol{x}$. For derivation of the S3T system (6) cf. Farrell and Ioannou (2003); Srinivasan and Young (2012).

The mean flow energy density, E_m, and the eddy energy density, E_p, are given as:

$$E_m = \int_\infty \mathrm{d}^2\boldsymbol{x}\,\frac{1}{2}\bar{u}^2\,, \tag{10a}$$

$$E_p = \int_\infty \mathrm{d}^2\boldsymbol{x}\,\frac{1}{2}\left[\,\overline{\boldsymbol{u}'_a\cdot\boldsymbol{u}'_b}\,\right]_{a=b} = -\int_\infty \mathrm{d}^2\boldsymbol{x}\,\frac{1}{4}\left[(\Delta_a^{-1}+\Delta_b^{-1})C\right]_{a=b}\,. \tag{10b}$$

[1]The mean vorticity flux can be written as: $\overline{v'\zeta'} = \langle v'\zeta'\rangle = \frac{1}{2}\langle v'_a\zeta'_b + v'_b\zeta'_a\rangle_{a=b}$ from which (9) follows.

where $\int_\infty \overset{\text{def}}{=} \lim_{L\to\infty}(2L)^{-2}\int_{-L}^{L}\int_{-L}^{L}$. The total averaged energy density relaxes over the dissipation scale (which is of $O(1)$ in the non-dimensional equations) to the energy supported under stochastic forcing and dissipation:

$$E(t) \overset{\text{def}}{=} E_m(t) + E_p(t) = \left[E(0) - \frac{\varepsilon}{2}\right] \mathrm{e}^{-2t} + \frac{\varepsilon}{2} \,. \qquad (11)$$

Therefore, the total energy remains bounded under S3T dynamics (Bakas and Ioannou 2015).

3. The jet-forming instability and the underlying eddy–mean flow dynamics

S3T dynamics under homogeneous stochastic forcing admit, for all parameter values, a homogeneous equilibrium with zero mean flow and homogeneous eddy covariance:

$$\bar{u}^e = 0 \;\;,\;\; C^e(\boldsymbol{x}_a - \boldsymbol{x}_b) = \frac{\varepsilon}{2} Q(\boldsymbol{x}_a - \boldsymbol{x}_b) \,. \qquad (12)$$

The homogeneous equilibrium state (12) becomes unstable at certain parameter values and bifurcates to inhomogeneous equilibria with mean flows in the form of *(i)* zonal jets (Farrell and Ioannou 2007; Bakas and Ioannou 2011; Srinivasan and Young 2012; Parker and Krommes 2013), *(ii)* waves traveling westward with speeds close to the corresponding Rossby wave speed (Bakas and Ioannou 2013a, 2014), or *(iii)* mean flows that consist of traveling waves embedded in jets (Bakas and Ioannou 2013a, 2014; Constantinou et al. 2016).

The mechanism underlying the jet-forming instability is discussed in detail by Bakas and Ioannou (2013b) and by Bakas et al. (2015). These studies investigated in detail which of the forced waves contribute to the instability in various parameter ranges. In this section, we review the main results regarding the instability of the homogeneous turbulent state to zonal jets and of the mechanism underlying it. In the following sections we use the framework developed by Bakas and Ioannou (2013b) and Bakas et al. (2015) to investigate in section 4 the role of each forced wave in the equilibration of the zonal jet instability.

To study the stability of the homogeneous state (12), we linearize (6) around (12). Since (12) is homogeneous, the eigenfunctions:

$$\delta\bar{u}(y)\,\mathrm{e}^{\sigma t} \quad \text{and} \quad \delta C(\boldsymbol{x}_a, \boldsymbol{x}_b)\,\mathrm{e}^{\sigma t} \,, \qquad (13a)$$

consist of a sinusoidal mean flow perturbation $\delta\bar{u}$ and a perturbation covariance δC with a sinusoidal inhomogeneous part:

$$\delta\bar{u} = \mathrm{e}^{\mathrm{i}ny} \;\;,\;\; \delta C = \tilde{C}_n^{(h)}(\boldsymbol{x}_a - \boldsymbol{x}_b)\,\mathrm{e}^{\mathrm{i}n(y_a+y_b)/2} \,, \qquad (13b)$$

where n is a real wavenumber that indicates the length-scale of the jets. The eigenvalues σ satisfy (see Appendix A):

$$\sigma + 1 = \varepsilon\, f(\sigma|\delta\bar{u}, Q/2) \,, \qquad (14)$$

where

$$f(\sigma|\delta\bar{u}, C) \overset{\text{def}}{=} \mathscr{R}\left[(\sigma + \mathscr{L})^{-1}\,\mathscr{N}(\delta\bar{u}, C)\right] \,, \qquad (15)$$

is the vorticity flux induced by the distortion of the incoherent homogeneous eddy equilibrium field with covariance $C^e = \varepsilon Q/2$ by the mean flow $\delta\bar{u}$. This induced vorticity flux is referred to as the *vorticity flux feedback on* $\delta\bar{u}$. If this vorticity flux feedback is positive[2], it has the tendency to reinforce the preexisting jet perturbation $\delta\bar{u}$ and therefore destabilizes it. With dissipation the critical parameter ε at which the homogeneous equilibrium becomes unstable to a mean flow jet with wavenumber n is

$$\varepsilon_t(n) \overset{\text{def}}{=} 1/f_r \,, \qquad (16)$$

assuming that the vorticity flux feedback

$$f_r \overset{\text{def}}{=} \mathrm{Re}\left[f(\sigma = 0|\delta\bar{u}, Q/2)\right] \,, \qquad (17)$$

is positive. For all values of β there is a minimum energy input rate

$$\varepsilon_c \overset{\text{def}}{=} \min_n[\varepsilon_t(n)] \,, \qquad (18)$$

above which the homogeneous state is unstable and jet formation occurs. Figure 1 shows the critical curves $\varepsilon_t(n)$ that separate stable from unstable homogeneous equilibria for three values of β. For $\varepsilon = \varepsilon_c$, only the jet with scale n_c is marginally unstable. For $\varepsilon > \varepsilon_c$, a band of wavenumbers neighboring n_c is also unstable.

It is instructive to identify which of the forced wave components of the incoherent flow contribute to the instability process. For the forcing spectrum (4) we may express the vorticity flux feedback at the stability boundary ($\sigma = 0$) as

$$f_r = \int_0^{\pi/2} \mathscr{F}(\vartheta, n)\,\mathrm{d}\vartheta \,, \qquad (19)$$

where $\mathscr{F}(\vartheta, n)$ is the contribution to f_r from the four waves with wavevectors $\boldsymbol{k} = (\pm\cos\vartheta, \pm\sin\vartheta)$ when the homogeneous equilibrium is perturbed by a sinusoidal jet perturbation with meridional wavenumber n. Angle ϑ measures the inclination of the wave phase lines with respect to the y-axis. The precise expression for $\mathscr{F}(\vartheta, n)$ is given in (A8) of Appendix A. Figures 2(a) and (b) show the contribution $\mathscr{F}(\vartheta, n)$ as a function of ϑ for the most unstable jet n_c for the cases with $\beta = 0.1$ and $\beta = 100$ and for isotropic forcing. Positive values of $\mathscr{F}$ indicate that waves with phase lines inclined at angle $|\vartheta|$ produce up-gradient vorticity fluxes and destabilize the jet perturbation n. In general, destabilizing vorticity fluxes are produced by waves with phase lines closely aligned to the y-axis (with small $|k_y|$).

When $\beta \ll 1$, $\mathscr{F}(\vartheta, n)$ is positive for angles satisfying $4\sin^2\vartheta < 1 + n^2$. This condition is derived for $\beta = 0$, but

[2]Note that for the ring forcing spectrum (4) both σ and $f(\sigma = 0|\delta\bar{u}, Q/2)$ are real for $n < 1$ (Srinivasan and Young 2012).

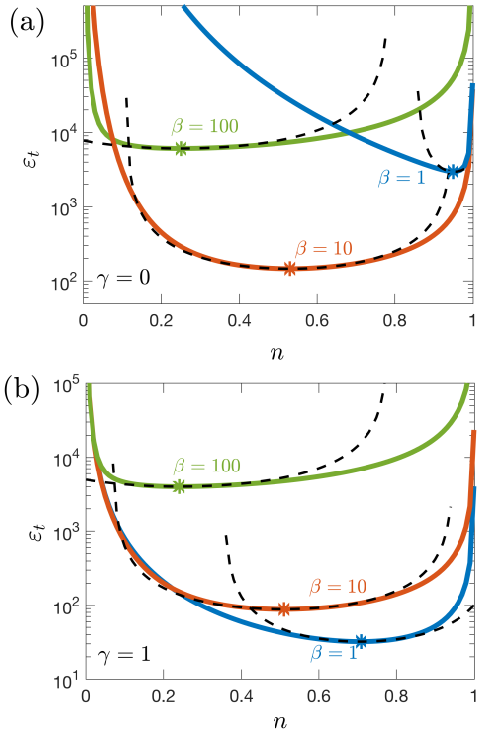

FIG. 1. The critical curves depicting the values of the energy input rate ε_t above which the homogeneous equilibrium is unstable as a function of the zonal jet perturbation wavenumber n. Shown are the critical curves for $\beta = 1$, 10 and 100 (solid curves). Panel (a) uses isotropic forcing ($\gamma = 0$) while panel (b) uses non-isotropic forcing ($\gamma = 1$). The asterisks mark the marginal points (n_c, ε_c). The dashed curves show the parabolic approximation (22) to the marginal curves obtained from the approximate eigenvalue relation (21) close to the marginal points (n_c, ε_c).

is also quite accurate for small β, as shown in figure 2(a) (Bakas et al. 2015). For isotropic forcing, the contribution from all angles is exactly zero up to first order in β. However, destabilization of the homogeneous equilibrium in this case occurs from the positive vorticity fluxes that are produced at order β^2 (Bakas and Ioannou 2013b). For anisotropic forcing with $\gamma > 0$, the net contribution from all orientations is destabilizing, even at $\beta = 0$, as waves at small angles are favorably excited.

For $\beta \gg 1$, only waves with phase lines almost parallel to the y axis ($k_y \approx 0$) contribute significantly to the vorticity fluxes (see figure 2). When integrated over all angles, the resulting vorticity flux feedback is positive and $O(\beta^{-2})$. The wave–mean flow dynamics underlying these contributions can be understood by considering the evolution of wave groups in the sinusoidal flow and were studied in detail by Bakas et al. (2015).

4. The Ginzburg–Landau (G–L) dynamics governing the nonlinear evolution of the jet-forming instability

In this section we discus how the equilibration of the zonal jet instabilities is achieved for the case just above the

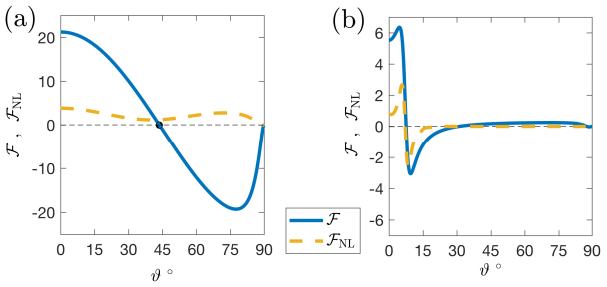

FIG. 2. The contribution $\mathscr{F}$ to the vorticity flux feedback f_r for the most unstable jet eigenfunction from the waves with phase lines inclined at angle ϑ with respect to the meridional (solid curves). Panel (a) shows the case with $\beta = 0.1$ while panel (b) for $\beta = 100$. In panel (a) the angle $\vartheta = \arcsin[\frac{1}{2}(1+n^2)^{1/2}]$ that separates the waves with positive (destabilizing) and negative (stabilizing) contribution to the vorticity flux feedback for $\beta = 0$ is indicated with the filled circle. Also, dashed curves show the contribution $\mathscr{F}_{\rm NL}$ to the nonlinear Landau coefficient c_3 for the most unstable jet eigenfunction as a function of the wave angle ϑ (see section 6). The forcing is isotropic ($\gamma = 0$).

critical threshold ε_c. To derive the asymptotic dynamics that govern the evolution of the jet amplitude we perform a multiple-scale perturbation analysis of the nonlinear dynamics near the marginal point. Before proceeding with the multiple-scale analysis we present an intuitive argument that suggests the appropriate slow time and slow meridional spatial scale for this problem.

a. The appropriate slow length scale and slow time scale

For a stochastic excitation with energy input rate $\varepsilon = \varepsilon_c$, zonal jets with wavenumber $n = n_c$ are marginally stable. If the energy input rate is slightly supercritical,

$$\varepsilon = \varepsilon_c(1+\mu^2)\,, \tag{20}$$

with $\mu \ll 1$, then zonal jets with wavenumbers $|n - n_c| = O(\mu)$ are unstable and grow at a rate of $O(\mu^2)$. To see this expand the eigenvalue relation (14) near ε_c:

$$\sigma = \mu^2 \varepsilon_c f_r + \varepsilon_c \left(\frac{\partial f}{\partial \sigma}\right)_c \sigma + \frac{\varepsilon_c}{2}\left(\frac{\partial^2 f}{\partial n^2}\right)_c (n-n_c)^2 + O\left[\sigma^2, (n-n_c)^3\right]\,, \tag{21}$$

where the subscript c denotes that the derivatives are evaluated at the threshold point $(\sigma, \mu, n) = (0, 0, n_c)$. Note that exactly at the minimum threshold $\varepsilon_c f_r = 1$ so that $\sigma = 0$. Since at the minimum threshold i.e. $\sigma = 0$, the function f has a minimum at $n = n_c$, term $(\partial f/\partial n)_c = 0$ and also $(\partial^2 f/\partial n^2)_c > 0$ (see Appendix B and figure 1). Thus the approximate eigenvalue relation (21) predicts that the locus of points of marginal stability ($\sigma = 0$) on the ε–n plane lie on the parabola:

$$(n-n_c)^2 = \frac{2}{|f_c''|}\left(\varepsilon/\varepsilon_c - 1\right) = \frac{2\mu^2}{|f_c''|}\,, \tag{22}$$

where $f_c'' \stackrel{\text{def}}{=} \partial^2 f/\partial n^2\big|_c$. The validity of the parabolic approximation of the marginal curve near the threshold is shown in figure 1 for various values of β. For large and small values of β, the parabolic approximation is only good in the neighborhood of the marginal point (ε_c, n_c). For intermediate values of β the parabolic approximation has a greater range of validity.

Using (21) we can estimate the growth rate σ at supercriticality (20). We find that jets with wavenumber $n = n_c + \mu\nu$ grow approximate at rate:

$$\sigma = \mu^2(1 - c_2\nu^2)/c_1 \,, \tag{23}$$

with

$$c_1 \stackrel{\text{def}}{=} 1 - \varepsilon_c \left(\frac{\partial f}{\partial \sigma}\right)_c \quad \text{and} \quad c_2 \stackrel{\text{def}}{=} \frac{\varepsilon_c}{2}|f_c''| \,. \tag{24}$$

The analytic expressions of c_1 and c_2 are given in (B13) and (B22). Both c_1 and c_2 are positive for stochastic excitations with spectrum (4). From (23), we deduce that for any given μ only jets with

$$|\nu| < \nu_e \stackrel{\text{def}}{=} 1/\sqrt{c_2} \,, \tag{25}$$

can become unstable. Equations (22) and (23) demonstrate the initial assertion: for $\mu \ll 1$ zonal jets with wavenumbers $|n - n_c| = O(\mu)$ grow at a rate $\sigma = O(\mu^2)$.

b. G–L dynamics for weakly supercritical zonal jets

To obtain the dynamics that govern weakly supercritical zonal flows consider the mean flow $\bar{u}$ and the covariance C of the S3T equations (6) expanded as:

$$\bar{u} = \mu\bar{u}_1(y,Y,T) + \mu^2\bar{u}_2(y,Y,T) + O(\mu^3) \,, \tag{26a}$$

$$C = C^e(\boldsymbol{x}_a - \boldsymbol{x}_b) + \mu\, C_1(\boldsymbol{x}_a, \boldsymbol{x}_b, Y_a, Y_b, T) + \mu^2 C_2(\boldsymbol{x}_a, \boldsymbol{x}_b, Y_a, Y_b, T) + O(\mu^3) \,. \tag{26b}$$

Guided by (22) and (23), we have assumed that the zonal jet and its associated covariance evolve from the marginal values at the slow time scale $T \stackrel{\text{def}}{=} \mu^2 t$, while being modulated at the long meridional scale $Y \stackrel{\text{def}}{=} \mu y$.

Details of the perturbation analysis are given in the Appendix B; here we present the backbone. We introduce (26) in (6) and gather terms with the same power of μ. At leading order μ^0, we recover the homogeneous equilibrium (12). At order μ^1, the emergent zonal jet and the covariance are the modulated S3T eigenfunction:

$$\bar{u}_1 = A(Y,T)\, \mathrm{e}^{\mathrm{i}n_c y} + \text{c.c.} \,, \tag{27a}$$

$$C_1 = \big[A(Y_a,T)\, G_c^+(0|\boldsymbol{x}_a - \boldsymbol{x}_b) - A(Y_b,T)\, G_c^-(0|\boldsymbol{x}_a - \boldsymbol{x}_b)\big]\, \mathrm{e}^{\mathrm{i}n_c(y_a+y_b)/2} + \text{c.c.} \,, \tag{27b}$$

with $G_c^{\pm}$ defined in (A4) and evaluated at $n = n_c$.

Having determined C_1 we proceed to determine the order μ^2 correction of the covariance, C_2. This step of the calculation is facilitated if we disregard the dependence on the slow spatial scale Y in the amplitude A, as well as that in C_1 and C_2. It is shown in Appendix B that with this simplification we obtain, without loss of generality, the terms of the asymptotic dynamics responsible for the equilibration of the amplitude A. The contribution to the asymptotic dynamics from the slow varying latitude Y is the addition of a diffusion term with the diffusion coefficient c_2 in (24). At order μ^2 a zonal jet with wavenumber $2n_c$ emerges:

$$\bar{u}_2 = \alpha_2 A(T)^2\, \mathrm{e}^{2\mathrm{i}n_c y} + \text{c.c.} \,, \tag{28a}$$

where α_2 is given in (B7). The associated covariance at order μ^2 is:

$$C_2 = C^e(\boldsymbol{x}_a - \boldsymbol{x}_b) + C_{20}(\boldsymbol{x}_a - \boldsymbol{x}_b, T) + C_{22}(\boldsymbol{x}_a - \boldsymbol{x}_b, T)\, \mathrm{e}^{2\mathrm{i}n_c(y_a+y_b)/2} + \text{c.c.} \,. \tag{28b}$$

It consists of the homogeneous part, $C^e + C_{20}$ and an inhomogeneous contribution at wavenumber $2n_c$. (Note that, as implied by (20), the forcing covariance Q appears order μ^0 and at order μ^2.)

The homogeneous covariance contribution, $C^e + C_{20}$, is required at order μ^2 so that the energy conservation (11) is satisfied. To show this note that as the instability develops on a slow time scale, the total energy density has already assumed (over an order one time scale) its steady state value $\varepsilon/2$ (see (11)) and therefore, the mean flow energy growth *must* be accompanied by a decrease in the eddy energy. This decrease is facilitated by a concomitant change of the eddy covariance at order μ^2. Specifically, by introducing perturbation expansion (26) in (11) at steady state, we obtain at leading order, μ^0, the trivial balance:

$$-\int_\infty \mathrm{d}^2\boldsymbol{x}\, \frac{1}{4}\left[(\Delta_a^{-1} + \Delta_b^{-1})C^e\right]_{a=b} = \frac{\varepsilon_c}{2} \,. \tag{29}$$

At order μ^1 the eddy covariance does not contribute to the energy since C_1 is harmonic in y and integrates to zero:

$$\int_\infty \mathrm{d}^2\boldsymbol{x}\, \frac{1}{4}\left[(\Delta_a^{-1} + \Delta_b^{-1})C_1\right]_{a=b} = 0 \,. \tag{30}$$

At order μ^2 we use *(i)* (29) and *(ii)* that the inhomogeneous component $C_{22}\, \mathrm{e}^{2\mathrm{i}n_c(y_a+y_b)/2}$ is also harmonic and integrates to zero, to obtain:

$$\int_\infty \mathrm{d}^2\boldsymbol{x}\, \frac{1}{4}\left[(\Delta_a^{-1} + \Delta_b^{-1})C_{20}\right]_{a=b} = \int_\infty \mathrm{d}^2\boldsymbol{x}\, \frac{1}{2}\bar{u}_1^2 \,. \tag{31}$$

Thus the homogeneous deviation from the equilibrium covariance must produce a perturbation energy *defect* to counter balance the energy growth of the mean flow. We refer to C_{20} as the *eddy energy correction term*.

At order μ^3 secular terms appear which, if suppressed, give us an asymptotic perturbation expansion up to time $O(1/\mu^2)$. Suppression of these secular terms requires that the amplitude A satisfies:

$$c_1\,\partial_T A = A - c_3 A|A|^2\,. \tag{32}$$

This gives us the evolution of the amplitude of the most unstable jet with wavenumber n_c. If we now allow the amplitude to evolve with the slow scale, Y, and adding the diffusion term $c_2\partial_Y^2 A$ on the r.h.s. of (32), we obtain the real Ginzburg–Landau (G–L) equation:

$$c_1\,\partial_T A = A + c_2\,\partial_Y^2 A - c_3 A|A|^2\,. \tag{33}$$

For forcing with spectrum (4) all three coefficients c_1, c_2, and c_3 are real and positive. The coefficients c_1 and c_2, are the coefficients in the Taylor expansion (21) and are given in (24).

The G–L equation (33) has a steady solution $A = 0$. This solution is linearly unstable to modal perturbations $\mathrm{e}^{\mathrm{i}\nu Y+\sigma T}$, with growth rate $\mu^2(1-\nu^2 c_2)/c_1$; the most unstable mode occurs at $\nu = 0$. This is the jet forming S3T instability of the homogeneous equilibrium state in the G–L framework (cf. (23)). The G–L equation has also the nonlinear harmonic equilibria

$$A(Y) = R_0(\nu)\,\mathrm{e}^{\mathrm{i}(\nu Y+\varphi)} \quad \text{with} \quad R_0(\nu) = \sqrt{(1-\nu^2 c_2)/c_3}\,, \tag{34}$$

with φ an undetermined phase that reflects the translational invariance of the system in y. These equilibria are the possible finite amplitude jets that emerge at low supercriticality. However, as will be shown in the next section some of these equilibria are susceptible to a secondary S3T instability and evolve through jet merging or jet branching to the subset of the stable attracting states.

The G–L equation obeys potential dynamics and thus the system always ends up in a stationary state which is a local minimum of the potential (Cross and Greenside 2009). The $\nu = 0$ jet is the state that corresponds to the global minimum of the potential and it has amplitude

$$R_0(0) = 1/\sqrt{c_3}\,. \tag{35}$$

It is interesting to note that even though G–L derives from a potential, one does not necessarily always get solutions that correspond to the absolute minimum of the potential.

5. Comparison of the predictions of G–L dynamics with S3T dynamics

In this section we test the validity of the weakly nonlinear G–L dynamics by comparing with fully nonlinear S3T simulation. As already noted by Parker and Krommes (2014), the quantitative accuracy of the approximation of the dynamics by the G–L equation is unfortunately limited only to parameter values that are very close to the stability boundary, i.e., only for $0 < \mu < 0.1$ (Parker and Krommes 2014). The reason is that the G–L equation is derived under the assumption of the approximate eigenvalue relation (21) near the critical value of the energy input rate ε_c, which is valid for most values of β only very close to the unstable wavenumber (cf. Fig. 1).

However, the G–L dynamics show qualitatively the same behavior as the S3T dynamics for low supercriticalities (up to $\mu \approx 0.5$) and reveals the dynamics of the secondary instabilities that some of the finite amplitude states are susceptible to. To show this, we present a comparison of the predictions of the fully nonlinear S3T dynamics and its approximation by G–L dynamics near the marginal point. We integrate the S3T dynamical system (6) in a doubly periodic domain $2\pi \times 2\pi$ and compare the evolution of the emerging jet with the corresponding evolution obtained from the G-L dynamics with periodic boundary conditions in the meridional. Due to the periodic boundary conditions in the jet amplitude A, a harmonic mean flow $A(Y,T)$ with wavenumber N corresponds to a mean flow in the doubly periodic box of the S3T system only if $N + n_c$ is integer. Therefore, we carefully choose the parameters ($k_f = 12$, $\beta = 11.77$, and $\gamma = 1$) so that the marginal wavenumber $n_c k_f$ assumes an integer value ($n_c k_f = 6$).

Figure 3 compares the evolution of the mean flow jet under S3T dynamics (6) (left panels) with the evolution of the mean flow jet as given by the G–L dynamics (33) (right panels) for supercriticality $\mu = 0.22$. The qualitative similarity is striking. For the parameters used the jet-forming instability of the homogeneous turbulent state first occurs for 6-jet mean flows; however at $\varepsilon/\varepsilon_c = 1.05$ the homogeneous state is also unstable to 5-jet and 7-jet states as well. We initialized both the S3T and the G–L integrations with the homogeneous turbulent equilibrium (12) perturbed with a mean flow consisting of a superposition of 5-jets and 6-jets mean state with the amplitude of the 5-jet mean flow perturbation being 10^7 times higher that the amplitude of the most unstable 6-jet mean flow perturbation. Initially, in both integrations the 5-jet mean flow grows at finite amplitude. However, under the G–L dynamics the finite-amplitude 5-jet state is secondarily unstable and thus it branches to the 6-jet state. This branching is also seen in the S3T integration. A similar integration with the 7-jet perturbation shows the 7-jet state growing, equilibrating and then transitioning into the 6-jet state through a secondary instability (not shown). This secondary instability of low supercriticality jets that is called Eckhaus instability and it is further discussed in section 7.

The G–L dynamics underestimates the amplitude of the equilibrated jet and the dynamic evolution times for the equilibration of the jet-forming and the secondary Eckhaus instabilities are different. This quantitative difference in the S3T and G–L predictions comes about because G–L dynamics crucially relies on a perturbation expansion about

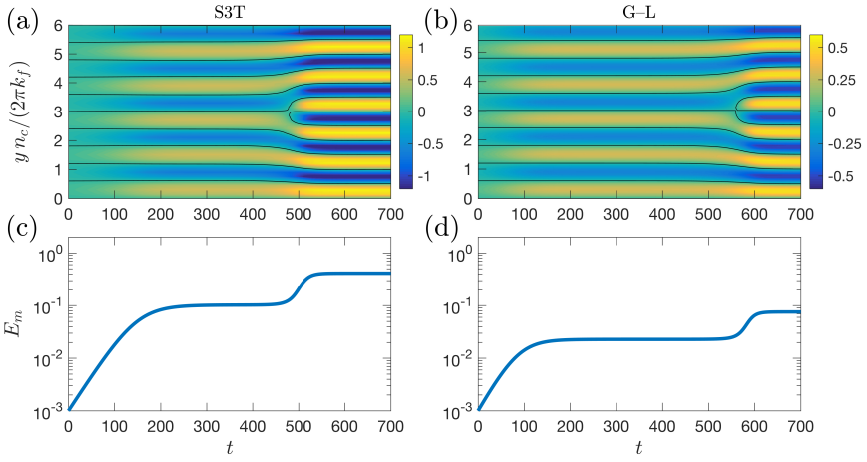

FIG. 3. Comparison of the evolution of mean flow, $\bar{u}(y,t)$, and the mean flow energy, $E_m(t)$, of an unstable 5-jet perturbation to the homogeneous state at $\varepsilon/\varepsilon_c = 1.05$, i.e., $\mu \approx 0.22$. Panels (a) and (c) show the predictions of the S3T dynamics and panels (b) and (d) the predictions of the G–L dynamics. Solid lines in panels (a) and (b) mark the $\bar{u} = 0$ contours. Simulations were performed in a domain of size $2\pi \times 2\pi$. Parameters: $k_f = 12$, $\beta = 11.77$, and $\gamma = 1$. For these parameters the homogeneous state (12) first becomes unstable when $\varepsilon_c = 94.2$ at the marginal wavenumber $n_c = 0.5$ that corresponds to 6 jets. The S3T simulation is initiated with the homogeneous state (12) perturbed by $\delta\bar{u} = \left[\sin(5y) + 10^{-7}\sin(6y)\right]/(5\sqrt{10})$. The same initial state is achieved in the G–L simulation using $A(Y,0) = -\mathrm{i}(\mathrm{e}^{-\mathrm{i}Y} + 10^{-7})/(5\sqrt{10})$. (The particular value of $\beta = 11.77$ was chosen so that $n_c k_f$ belongs in the set of allowed wavenumbers that fit the $2\pi \times 2\pi$ domain.)

the marginal point (ε_c, n_c). As we move away from that point (both by increasing ε and by considering mean flows with length scale other than the critical n_c) the assumptions used to obtain the G–L dynamics begin to fail. However, the qualitative agreement between the predictions of the G–L dynamics and the predictions of the S3T dynamics regarding the equilibration of the jet-forming instability demonstrates that the underlying dynamics that govern the equilibration of the jet-forming instability at low supercriticalities are exactly those described by G–L (33) dynamics. Therefore, in the following sections we use the G–L dynamics to study the physical processes that underly the finite amplitude equilibration of the jets as well as the incipient secondary instabilities involved.

6. The physical processes underlying the equilibration of the S3T instability of the homogeneous state

One of the main objectives of this paper is the study of the nonlinear term in the G–L (33), with coefficient c_3, that controls the halting of the jet-forming instability. We first discuss the dependence of c_3, and consequently of the equilibration amplitude $R_0(0)$, on β. Figure 4 shows the amplitude of the most unstable jet, $R_0(0)$, as a function of β. For $\beta \gg 1$ the emerging jets have large scales, as shown in figure 1, and equilibrate with amplitude that increases as $R_0 \sim \beta^{1/3}$. This asymptotic behavior applies to both isotropic or anisotropic excitation. For $\beta \ll 1$, the emerging jets have small scales and their amplitude depends on the structure of excitation: for anisotropic forcing ($\gamma = 1$) the equilibrium amplitude asymptotes to a value which is independent of β, while for isotropic forcing ($\gamma = 0$) the equilibration amplitude decreases as $R_0 \sim \beta^{2/3}$.

The dependence of the amplitude $R_0(0)$ on β can be understood by considering the contribution of the various wave components to c_3, in a similar manner as we did for f_r in (19). Thus we write:

$$c_3 = \int_0^{\pi/2} \mathscr{F}_{\mathrm{NL}}(\vartheta)\,\mathrm{d}\vartheta\ , \tag{36}$$

where $\mathscr{F}_{\mathrm{NL}}$ is the contributions to c_3 from the four waves with wavevectors $\boldsymbol{k} = (\pm\cos\vartheta, \pm\sin\vartheta)$. Figure 2 shows the contributions $\mathscr{F}_{\mathrm{NL}}(\vartheta)$ for two values of β.

For $\beta \ll 1$, all wave orientations contribute positively to c_3. As a result, the up-gradient contributions to the vorticity flux feedback $\mathscr{F}$ at small ϑ are counteracted by $\mathscr{F}_{\mathrm{NL}}$, while the down-gradient contributions to $\mathscr{F}$ at higher ϑ are enhanced by $\mathscr{F}_{\mathrm{NL}}$. This leads to a rapid quenching of the instability and thus to a weak finite amplitude jet.

For large β, $\mathscr{F}_{\mathrm{NL}}$ has roughly the same dipole structure centered about an angle ϑ_0 as the vorticity flux feedback $\mathscr{F}$. Therefore, only waves with angles close to ϑ_0 contribute appreciably to c_3. Waves with at angles $|\vartheta| < \vartheta_0$ give positive contributions to c_3, while waves with angles $|\vartheta| > \vartheta_0$ give negative contributions to c_3. As a result, both the up-gradient and the down-gradient contributions to $\mathscr{F}$ are almost equally reduced and the instability is only slowly hindered and is allowed to drive jets with a much larger amplitude compared to $\beta \ll 1$. To understand the power law increase of $R(0)$ with β, note that as β increases: *(i)* the heights of the dipole peaks grow linearly with β, *(ii)* the widths of the dipole peaks decrease as $\beta^{-2/3}$, and

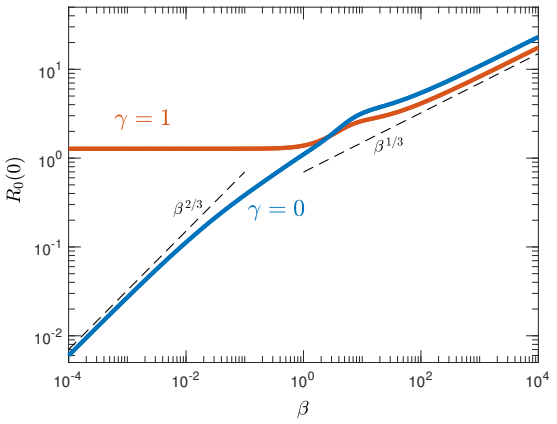

FIG. 4. The amplitude $R_0(0) = 1/\sqrt{c_3}$ of the equilibrated most unstable jet with wavenumber n_c as a function of β for the case with isotropic ($\gamma = 0$) and anisotropic ($\gamma = 1$) forcing. Dashed lines show the $\beta^{1/3}$ and $\beta^{2/3}$ slopes for reference.

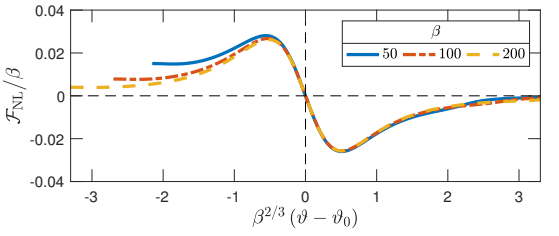

FIG. 5. The contribution $\mathscr{F}_{\rm NL}$ to the coefficient c_3 from waves at angle $|\vartheta|$ in the limit of $\beta \gg 1$. $\mathscr{F}_{\rm NL}$ assumes a dipole pattern. The amplitude of each of the dipole peaks scale with β and the widths of the dipole structure scale with $\beta^{-2/3}$. In the $\beta \gg 1$ limit the structure of $\mathscr{F}_{\rm NL}$ is independent of the type of forcing used. Here, isotropic forcing ($\mu = 0$) was used.

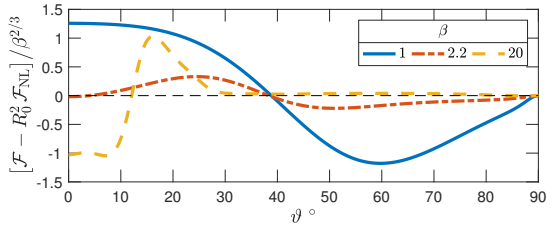

FIG. 6. The contribution from waves at angle $|\vartheta|$ to the finite amplitude equilibrium jet, as given by $\mathscr{F} - R_0^2\mathscr{F}_{\rm NL}$ for three values of β. Plot shows results for isotropic forcing ($\mu = 0$); similar qualitative behavior also occurs for anisotropic forcing (not shown).

(iii) the structure of dipole becomes more symmetric about ϑ_0. Figure 5 demonstrates points *(i)-(iii)*. Thus, each of the positive and the negative contribution to c_3 scale as $\beta \times \beta^{-2/3} = \beta^{1/3}$ and their difference scales with the derivative, i.e., as $\mathrm{d}\beta^{1/3}/\mathrm{d}\beta \propto \beta^{-2/3}$ leading to the increase of $R(0)$ with β as $\beta^{1/3}$.

We then investigate how each of the forced waves contribute in sustaining the equilibrated state of the most unstable jet ($\nu = 0$) with amplitude $R_0(0)$ by decomposing the portion of the vorticity flux exceeding dissipation which is the sum of f_r and $-c_3 R_0(0)^2$, into contributions from various wave angles:

$$f_r - c_3 R_0(0)^2 = \int_0^{\pi/2} \left[\mathscr{F}(\vartheta) - R_0^2 \mathscr{F}_{\rm NL}(\vartheta)\right] \mathrm{d}\vartheta \ . \quad (37)$$

Figure 6 shows these contributions for three values of β. For small values of β waves with angles $|\vartheta| < \pi/4$ that drive the instability through their up-gradient contribution also support the equilibrated jet. However, for $\beta \gg 1$ this picture is reversed. The instability is driven by waves with $|\vartheta| < \vartheta_0$ (mainly from waves with $|\vartheta| \approx 0$) and is hindered by waves with angles $|\vartheta| > \vartheta_0$, while the equilibrated jet is supported through the up-gradient fluxes of waves with angles $|\vartheta| > \vartheta_0$. The reason is the the amplitude $R_0(0)$ is so large that the sign of the integrand in (37) is reversed.

Further intuition into the equilibration dynamics can be gained by noting that the coefficient c_3 can be written as the sum of three separate contributions:

$$c_3 = c_3^{ec} + c_3^{f12} + c_3^{f21} \ , \quad (38)$$

each of which represents a different physical process (details on the decomposition can be found in Appendix B). These contributions correspond to the three $O(\mu^3)$ possible interactions between the perturbed components of the mean flow $\mu\bar{u}_1$ and $\mu^2\bar{u}_2$ with the covariance corrections μC_1, $\mu^2 C_{20}$, $\mu^2 C_{22}$.

Coefficient

$$c_3^{ec} \propto -f\,(0\,|\,\bar{u}_1, C_{20}) \ , \quad (39)$$

is proportional to the mean vorticity flux feedback from the interaction of $\mu\bar{u}_1$ with the homogeneous covariance correction $\mu^2 C_{20}$ to the equilibrium C^e. It measures the compensation in the vorticity flux as perturbations loose energy to the mean flow.

Coefficient

$$c_3^{f12} \propto -f\left(0\,\middle|\,\bar{u}_1, C_{22}\,\mathrm{e}^{2\mathrm{i}n_c(y_a+y_b)/2} + \mathrm{c.c.}\right) \ , \quad (40)$$

measures the mean vorticity flux feedback from the interaction of $\mu\bar{u}_1$ with the inhomogeneous covariance correction $\mu^2 C_{22}\,\mathrm{e}^{2\mathrm{i}n_c(y_a+y_b)/2}$ to the equilibrium C^e.

Coefficient

$$c_3^{f21} \propto -f\,(0\,|\,\bar{u}_2, C_1) \ . \quad (41)$$

measures the mean vorticity flux feedback from the interaction of $\mu^2\bar{u}_2$ with the inhomogeneous covariance correction μC_1 to the equilibrium C^e. The exact form of all three coefficients is given in (B16), (B18), and (B20) respectively.

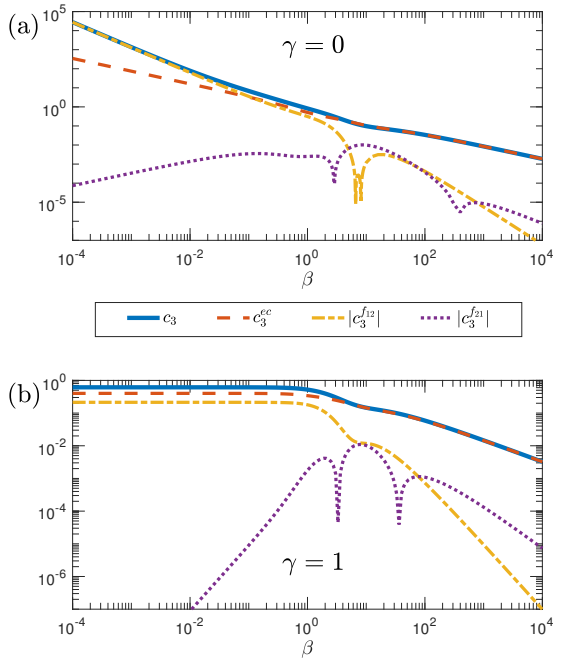

FIG. 7. The coefficient c_3 and its decomposition into the various contributions c_3^{ec}, $c_3^{f_{12}}$, and $c_3^{f_{21}}$, as a function of β. Panel (a) uses isotropic forcing ($\gamma = 0$) and panel (b) anisotropic forcing ($\gamma = 1$). (Coefficient $c_3^{f_{12}}$ becomes negative for $6.6 \lessapprox \beta \lessapprox 8.1$ when $\gamma = 0$; coefficient $c_3^{f_{21}}$ becomes negative for $2.9 \lessapprox \beta \lessapprox 398.1$ when $\gamma = 0$ and for $3.3 \lessapprox \beta \lessapprox 36.3$ when $\gamma = 1$. However, in these ranges of β both of these contributions are at least an order of magnitude less than c_3^{ec} and, therefore, negligible.)

We then analyze the contribution of the three processes in c_3 in figure 7 as a function of β. We observe that the main contribution to the coefficient c_3 comes from c_3^{ec} for most values of β. Only for $\beta \ll 1$ is there a contribution from $c_3^{f_{12}}$ at the same order and further analysis of the eddy correction feedback and the feedback resulting from the interaction of the emerging zonal jet flow, $\bar{u}_1$, with the inhomogeneous covariance C_{22}, reveals that there are similar contributions of the eddies to these feedbacks in this limit. We can therefore conclude that the mean flow is stabilized by the reduction of the eddy energy brought by total energy conservation that leads to a concomitant reduction of the up-gradient fluxes. For $\beta \ll 1$ there is no change in the eddy–mean flow dynamical processes involved, while for $\beta \gg 1$ the equilibrated flow is supported by the up-gradient fluxes of the eddies that were initially hindering its formation.

7. Eckhaus instability of the finite amplitude jets and phase dynamics

Based on the G–L dynamics (33) we address in this section the stability of the inhomogeneous statistical jet equilibria with zonal jet amplitude given by (34). As noted by Parker and Krommes (2014), the harmonic jet equilibria are susceptible to Eckhaus instability, a well known result for harmonic equilibria of the G–L equation (Hoyle 2006). Here, we present the main results of the Eckhaus instability and interpret them in terms of the interaction between the turbulent eddies and the emerged jet.

a. An intuitive view of the Eckhaus instability

To obtain an intuition for the eddy–mean flow dynamics underlying the Eckhaus instability, note first that the G–L dynamics are given by the balance between the vorticity flux feedback $f_r(\nu) = f_r(0) - c_2\nu^2$, which provides a diffusive correction to the original up-gradient fluxes $f_r(0) > 0$ at n_c, and the stabilizing nonlinear term $c_3|A|^2$. Let us assume an equilibrium jet with $\nu > 0$, i.e. with a scale smaller than that of the most unstable jet at n_c, and also assume a sinusoidal phase perturbation:

$$A(Y) = R_0\, e^{i[\nu Y + \eta \sin(qY)]} \quad \text{with} \quad \eta \ll 1 \,. \tag{42}$$

Figure 8 shows how the perturbed jet (42) is compressed for half the wavelength of the phase perturbation π/q (unshaded region) and dilated for the other half (shaded region). In the compressed region the jet appears with an enhanced wavenumber $\nu + \delta\nu$ while in the dilated region the jet appears with a reduced wavenumber $\nu - \delta\nu$. As a result, the vorticity flux feedback $f_r(\nu)$ is larger in the dilated (shaded) region implying a tendency to enhance the jet; the opposite occurs in the compressed region (non-shaded). In figure 8 a qualitative sketch of the mean vorticity fluxes, $\overline{v'\zeta'}$, demonstrates this process. If the nonlinear term does not counteract this mismatch, the dilated part of the jet will grow and take over the whole domain thus producing a jet with lower ν. (Similarly, for an equilibrium jet with $\nu < 0$ there is a tendency for the compressed part of the jet to take over the whole domain producing a jet with larger ν.)

To summarize, due to the diffusive nature of the vorticity flux feedback there is a tendency to go to towards $\nu = 0$ jets if not counteracted by the nonlinear eddy–mean flow feedback.

b. A formal view of the Eckhaus instability

To address quantitatively the stability of the harmonic jet equilibria (34), let us reformulate the G–L equation by rewriting the jet amplitude A in polar form as:

$$A(Y,T) = R(Y,T)\, e^{i\Theta(Y,T)} \,, \tag{43}$$

where R is the amplitude and Θ is the phase of the jet. Substituting (43) into (33) and separating real and imaginary parts we obtain:

$$c_1\partial_T R = \left[1 + c_2\partial_Y^2 - c_2(\partial_Y\Theta)^2\right] R - c_3R^3 \,, \tag{44a}$$

$$c_1R\partial_T\Theta = 2c_2(\partial_Y R)(\partial_Y\Theta) + c_2R\partial_Y^2\Theta \,. \tag{44b}$$

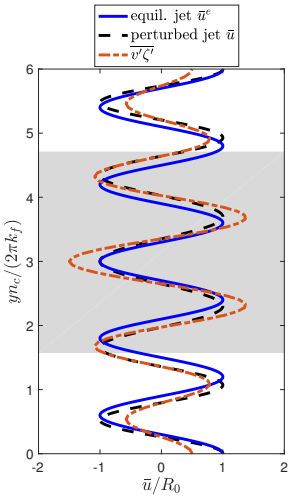

FIG. 8. A sinusoidal equilibrium jet $\bar{u}^e = R_0\cos(\nu y)$ (solid) with larger scale $\nu = 5n_c/6$ compared to the scale of the most unstable jet (the wavenumber differences with the most unstable jet are exaggerated here for illustration purposes). Shown with a dashed curved is the jet that results when the phase of the equilibrium jet $\bar{u}^e$ is perturbed: $\bar{u} = R_0\cos[\nu y + \eta\sin(qy)]$, with $q = \nu/5$. This perturbation dilates the jet in the shaded region and compresses the jet in the unshaded region. A qualitative depiction of the expected vorticity flux feedback $\overline{v'\zeta'}$ for the perturbed jet based on the dependence of f_r on the wavenumber ν is also shown (dash-dotted).

Assume now an equilibrium jet with constant amplitude $R_0(\nu)$ given by (34) and a linearly varying phase $\Theta = \nu Y$. From (25), such equilibria exist only for $|\nu| < \nu_e = \sqrt{1/c_2}$. Consider small perturbations about this equilibrium jet:

$$R = R_0(\nu) + \rho \quad \text{and} \quad \Theta = \nu Y + \phi \ , \tag{45}$$

and linearize (44) to obtain:

$$c_1\partial_T\rho = \left[1 + c_2(\partial_Y^2 - \nu^2) - 3c_3R_0^2\right]\rho - 2c_2R_0\nu\partial_Y\phi \ , \tag{46a}$$

$$c_1R_0\partial_T\phi = 2c_2\nu\partial_Y\rho + c_2R_0\partial_Y^2\phi \ . \tag{46b}$$

Perturbations of the form $[\rho,\phi] = [\hat{\rho},\hat{\phi}]e^{iqY+\lambda T}$ are eigenmodes of (46) when:

$$\lambda = \frac{\nu^2 - \nu_e^2 - q^2 \pm \sqrt{(\nu^2-\nu_e^2)^2 + 4q^2\nu^2}}{c_1\nu_e^2} \ . \tag{47}$$

Instability occurs for $q^2 > 2(3\nu^2 - \nu_e^2)$, i.e. equilibria (45) with $|\nu| > \nu_e/\sqrt{3}$ are Eckhaus unstable. Maximum instability occurs for

$$|q|_{\max} = \nu_e\frac{\sqrt{3(\nu/\nu_e)^4 + 2(\nu/\nu_e)^2 - 1}}{2(\nu/\nu_e)} \ . \tag{48}$$

Figure 9(a) shows the wavenumber $|q|_{\max}$ as a function of the equilibrium jet wavenumber ν. Note that the equilibria with wavenumbers $\nu \approx \nu_e/\sqrt{3}$ are unstable to jets with neighboring wavenumbers as $|q|_{\max} \ll 1$, while equilibria with wavenumbers $\nu \approx \nu_e$ are unstable to the jet with wavenumber n_c as $|q|_{\max} \approx 1$.

The growth rate for the most unstable structure with $|q|_{\max}$ is

$$\lambda_{\max} = \frac{(3\nu^2 - \nu_e^2)^2}{4c_1\nu_e^2\nu^2} \ . \tag{49}$$

Figure 9(b) shows $\lambda_{\max}$ as a function of the equilibrium jet wavenumber ν. The Eckhaus instability will form a jet of wavenumber $n_c + \mu(\nu \pm |q|_{\max})$. Note that the growth rate of the Eckhaus instability is, for almost all wavenumbers ν, much less than the corresponding growth rate of the jet-forming instability of the homogeneous state of a jet at $n_c + \mu(\nu \pm |q|_{\max})$ (shown with dashed curve in figure 9(b)). Consequently, the slow Eckhaus instability manifests only in carefully contrived S3T integrations; any integration of the full S3T system (6) starting from a random initial perturbation will evolve at low supercriticality into the most unstable jet with wavenumber n_c which is the global attracting point of the G–L equation.

FIG. 9. Panel (a) shows the most unstable wavenumber for the Eckhaus instability, $|q|_{\max}/\nu_e$, as a function of the jet equilibrium wavenumber ν/ν_e. Instability occurs in the shaded region for $\nu/\nu_e > 1/\sqrt{3}$. Panel (b) shows with solid curvet the growth rate for the most Eckhaus unstable jet with $q = q_{\max}$ (49) as a function of the jet equilibrium wavenumber ν. Also shown with dashed curve is the corresponding growth rate for the jet-forming instability of the jet with wavenumber $\nu \pm q_{\max}$ that will eventually be formed by the Eckhaus instability and is given by $\left[1 - (\nu \pm q_{\max})^2/\nu_e^2\right]/c_1$, according to the G–L equation (33).

This stability analysis can be related to the wave–mean flow interactions discussed in the beginning of this section, by assuming a slow phase and amplitude variation $q \ll 1$, as in figure 8. In this case the negative eigenvalue is of $O(1)$ with eigenvector $[\hat{\rho},\hat{\phi}] = [1, O(q/\nu_e)]$, while the unstable eigenvalue is of $O[(q/\nu_e)^2]$ with eigenvector $[\hat{\rho},\hat{\phi}] = [O(q/\nu_e), 1]$. That is, the perturbation amplitude ρ relaxes quickly towards $O(q/\nu_e)$ values while the perturbation phase ϕ grows slowly. To examine the behavior of the linearized dynamics in this case, consider the spatial derivatives in the perturbation equations (46) to be of order $q = \delta \ll 1$ and the perturbations to evolve according to the slow time scale of order δ^2. Then, (46) become:

$$c_1\delta^2\partial_T\rho = \left[1 + c_2(\delta^2\partial_Y^2 - \nu^2) - 3c_3R_0^2\right]\rho - 2c_2R_0\nu\delta\partial_Y\phi \ , \tag{50a}$$

$$c_1R_0\delta^2\partial_T\phi = 2c_2\nu\delta\partial_Y\rho + c_2R_0\delta^2\partial_Y^2\phi \ . \tag{50b}$$

From (50a) and using (34), we obtain that to leading order the amplitude instantaneously adjusts to

$$\rho = -\delta\frac{\nu\partial_Y\phi}{c_3R_0\nu_e^2} \ . \tag{51}$$

Thus, the sinusoidal phase variation of figure 8 drives an amplitude change that is negative in the shaded region

and positive in the unshaded region; consistent with the discussion in the beginning of this section. Notice also, that the equilibration in the amplitude results from the balance of the reduced vorticity flux feedback term and the nonlinear term (which is the sum of the first and last terms in the G–L equation (33)). Substituting the amplitude in the phase equation (50b) we obtain:

$$c_1 \partial_T \phi = -\frac{2\nu^2}{c_3 R_0^2 \nu_e^4} \partial_Y^2 \phi + c_2 \partial_Y^2 \phi \ . \tag{52}$$

This implies a diffusion of phase (the second term on r.h.s. in (52)) that results from the diffusion term $\partial_Y^2 A$ in the G–L equation, and an anti-diffusion of phase (the first term on r.h.s. in (52)) that results from the mismatch in the vorticity flux feedback between the dilated and the compressed part of the jet. Eckhaus instability arises when the anti-diffusion term overcomes the diffusion term.

8. Discussion – Conclusion

We examined the dynamics that underly the formation and support of zonal jets at finite amplitude in forced–dissipative barotropic beta-plane turbulence using the statistical state dynamics of the turbulent flow closed at second-order. Within this framework, jet formation is shown to arise as an instability of the homogeneous statistical equilibrium state when the energy input rate of the stochastic forcing passes a certain critical threshold. In this work, we studied the dynamics underlying the equilibration of the jet-forming instability in the limit of small supercriticality.

In this limit, we used a two-time two-scale approximation to derive the weakly nonlinear Ginzburg–Landau dynamics that governs the evolution of the zonal jet. We investigated in section 5 the accuracy of the weakly nonlinear G–L dynamics (33) through comparison with fully nonlinear simulations of the S3T dynamical system. The quantitative predictions of G–L dynamics quickly depart from those of the fully nonlinear S3T dynamics (6); for example, for superciticality as low as $\mu \approx 0.25$ we have that the G–L dynamics underestimate the final amplitude of the equilibrated jets roughly by 50%. However, G–L dynamics capture all of the qualitative characteristics of the equilibration of jet-forming instability at low supercriticality and, as a result, this allows us to gain intuition for the equilibration processes though the much simpler G–L dynamics.

The coefficients in the G–L equation were derived in a physically intuitive way that allows the investigation of the physical processes underlying the eddy–mean flow dynamics responsible for the equilibration process and maintenance of the jet at finite amplitude. Using the methods of Bakas et al. (2015) we separated the contributions of the various eddies in the induced vorticity fluxes: both for the linear term in the G–L equation that drives the instability, and also for the nonlinear term that stabilizes the flow. This way, we identified which of the eddies yield up-gradient fluxes and which of the eddies yield down-gradient fluxes and, furthermore, how the up-gradient or down-gradient character of the fluxes changes as the jet grows.

The central physical process responsible for the equilibration of the S3T jet-forming instability at small supercriticality is the reduction in the up-gradient vorticity flux that occurs as the initially unstable eddy field transfers energy to the emergent jet. The equilibration also depends on the non-dimensional parameter $\beta_* = \beta/(k_f r)$.

For low values of β_*, the instability is quickly quenched and the jets equilibrate at low amplitude. The reason is that the contribution of the eddies that induce up-gradient fluxes and drive the instability is weakened as the jets emerge while simultaneously the contribution of the eddies that induce down–gradient fluxes is increased (eddies with phase lines forming a small angle with respect to the meridional are up-gradient; otherwise they are down-gradient). As a result, the jets equilibrate at a small amplitude and are supported by the same eddies that drive the instability. The asymptotic amplitude of the jet for small β_* decreases as $\beta_*^{2/3}$ for isotropic forcing (with no jets at emerging at $\beta_* = 0$) while the jet amplitude approaches a constant non-zero amplitude that is independent of β_* when the forcing is anisotropic.

For large values of β_*, both the up-gradient and the down-gradient contributions are almost equally weakened thus leading to a slow decay of the growth rate and to an equilibrated jet with a much larger amplitude that asymptotically reaches $\beta_*^{1/3}$. Because the equilibrium amplitude is large, the stabilizing fluxes that are multiplied by the square of the jet amplitude in the G–L equation are dominant and, therefore, at equilibrium the jet is supported by the eddies that were initially hindering its growth (these eddies have phase lines that form small angles with the meridional but different than zero).

Furthermore, we studied the stability of finite amplitude jets which are single harmonics (cf. (34)). Zonal jets with scales close to the scale n_c of the most unstable mode of the jet-forming instability are stable; jets with scales much larger or much smaller are unstable. The incipient Eckhaus instability is well studied within the pattern formation literature and here it was interpreted in a physically intuitive way. The equilibrated jets have a low amplitude (proportional to the supercriticality) and therefore do not significantly change the structure of the turbulence. As a result, a mean flow perturbation on the turbulent flow induces approximately the same vorticity flux feedback as in the absence of any jet with the vorticity flux feedback having a maximum at the most unstable wavenumber. Therefore, when a dilation–compression phase perturbation is inserted in the equilibrated jet that has a different wavenumber than n_c, either the dilated or the compressed part of the jet tends to grow and take over the whole domain resulting in a

jet with scale close to n_c regardless of the supercriticality. The growth of the phase of the perturbation occurs anti-diffusively (cf. (51)). The Eckhaus instability evolves at a much slower rate than the jet-forming instability, and thus it does not appear in S3T simulations unless carefully set up.

A future study will address the dynamics responsible for the equilibration of jets at high supercriticalities. In this limit, the secondary instabilities have an important qualitative difference compared to the Eckhaus instability: as superciticality increases, mean flow–turbulence states with finite amplitude jets undergo an S3T instability and typically transition to equilibria with ever larger-scale jets (Farrell and Ioannou 2007; Constantinou et al. 2014a; Constantinou 2015). This is different from the of the weak jets in this study that either merge or branch to reach a scale close to n_c. However, based on the relevant dynamics in pattern formation, we expect that the anti-diffusive phase dynamics involved in the Eckhaus instability will play a significant role in the secondary instabilities of large-amplitude jets as well.

Acknowledgments. The authors would like to thank Jeffrey B. Parker for helpful comments. N.A.B. was supported by the AXA Research Fund. N.C.C. was partially supported by the NOAA Climate and Global Change Postdoctoral Fellowship Program, administered by UCAR's Cooperative Programs for the Advancement of Earth System Sciences.

APPENDIX A

Eigenvalue relation of the jet-forming instability

In this appendix we derive the eigenvalue relation of the jet-forming instability. The eigenvalue relation was first derived by Srinivasan and Young (2012). Here, however, we repeat the derivation mainly to introduce some notation and terminology that will prove to be helpful in understanding the nonlinear equilibration of the jet-forming instability.

The eigenvalue relation is obtained by linearizing the S3T system (6) about the homogeneous equilibrium (12). Introducing the ansantz (13) in the linearized S3T system we obtain:

$$(\sigma+1)\delta\bar{u} = \mathscr{R}(\delta C)\,, \tag{A1a}$$

$$\delta C = (\sigma+\mathscr{L})^{-1}\,\mathscr{N}(\delta\bar{u}, C^e)\,. \tag{A1b}$$

The inversion of the operators and the algebra is simplified by taking the Fourier decomposition of $\tilde{C}_n^{(h)}$:

$$\tilde{C}_n^{(h)}(\boldsymbol{x}_a-\boldsymbol{x}_b) = \int \frac{\mathrm{d}^2\boldsymbol{k}}{(2\pi)^2}\,\hat{C}(\boldsymbol{k})\,\mathrm{e}^{\mathrm{i}\boldsymbol{k}\cdot(\boldsymbol{x}_a-\boldsymbol{x}_b)}\,. \tag{A2}$$

By inserting (A2) and (12) into (A1b) we obtain:

$$\delta C = \varepsilon\,\mathrm{e}^{\mathrm{i}n(y_a+y_b)/2}\left[G^+(\sigma,\boldsymbol{x}_a-\boldsymbol{x}_b) - G^-(\sigma|\boldsymbol{x}_a-\boldsymbol{x}_b)\right]\,, \tag{A3}$$

where we defined

$$G^{\pm}(\sigma|\boldsymbol{x}) \overset{\text{def}}{=} \int \frac{\mathrm{d}^2\boldsymbol{k}}{(2\pi)^2}\,\frac{\mathrm{i}k_x k_{\mp}^2(k_{\pm}^2-n^2)}{(\sigma+2)k_+^2k_-^2+2\mathrm{i}\beta n k_x k_y}\,\frac{\hat{Q}(\boldsymbol{k}_{\pm})}{2}\mathrm{e}^{\mathrm{i}\boldsymbol{k}\cdot\boldsymbol{x}}\,, \tag{A4}$$

with $\boldsymbol{k}_{\pm}=\boldsymbol{k}+\boldsymbol{n}/2$, $\boldsymbol{n}=(0,n)$ and $k_{\pm}=|\boldsymbol{k}_{\pm}|$. Inserting (A3) in (A1a) we obtain (14), in which

$$f = \int \frac{\mathrm{d}^2\boldsymbol{k}}{(2\pi)^2}\,\frac{nk_x^2(k_y+n/2)\,(1-n^2/k^2)}{(\sigma+2)k^2k_s^2+2\mathrm{i}\beta n k_x(k_y+n/2)}\,\hat{Q}(\boldsymbol{k})\,, \tag{A5}$$

where $k_s \overset{\text{def}}{=} |\boldsymbol{k}+\boldsymbol{n}|$. After substituting the ring forcing power spectrum (4), expressing the integrand in polar coordinates $(k_x,k_y)=(k\cos\vartheta, k\sin\vartheta)$ and integrating over k (A5) becomes:

$$f = \int_0^{2\pi} \frac{N_f\,\mathrm{d}\theta}{(\sigma+2)D_f+\mathrm{i}\beta D_\beta}\,, \tag{A6}$$

with $N_f(\theta) = n\cos^2\theta(\sin\vartheta+n/2)(1-n^2)\,[1+\gamma\cos(2\vartheta)]/\pi$, $D_f(\vartheta)=\cos^2\vartheta+(\sin\vartheta+n)^2$ and $D_\beta(\vartheta) = 2n\cos\vartheta(\sin\vartheta+n/2)$. At criticality ($\sigma=0$), using the mirror symmetry property of the forcing, i.e. $\hat{Q}(-k_x,k_y)=\hat{Q}(k_x,k_y)$, the vorticity flux feedback is rewritten as:

$$f_r = \int_0^{\pi/2} \mathscr{F}(\vartheta,n)\,\mathrm{d}\vartheta\,, \tag{A7}$$

where

$$\mathscr{F}(\vartheta,n) = \frac{N_f(\vartheta)D_f(\vartheta)}{4D_f^2(\vartheta)+\beta^2D_\beta^2(\vartheta)} + \frac{N_f(\vartheta+\pi)D_f(\vartheta+\pi)}{4D_f^2(\vartheta+\pi)+\beta^2D_\beta^2(\vartheta+\pi)}\,, \tag{A8}$$

is the contribution to the feedback from the waves with wavevectors (k_x,k_y), $(-k_x,-k_y)$ and their mirror symmetric $(-k_x,k_y)$ and $(k_x,-k_y)$ respectively.

APPENDIX B

Ginzburg–Landau equation for the weakly nonlinear evolution of a zonal jet perturbation about the homogeneous state

To obtain the G–L equation governing the nonlinear S3T dynamics near the onset of the instability, we assume that the energy input rate is slightly supercritical $\varepsilon = \varepsilon_c(1+\mu^2)$, where $\mu \ll 1$ measures the supercriticality. As discussed in section 4, the emerging jet grows slowly at a rate $O(\mu^2)$ and contains a band of wavenumbers of $O(\mu)$ around n_c, where n_c is the wavenumber of the jet that achieves neutrality at ε_c. Therefore, we assume that the dynamics evolve on a slow time scale $T = \mu^2 t$ and are modulated at a long meridional scale $Y = \mu y$. The leading order jet is $\bar{u}_1 = A(Y,T)\,\mathrm{e}^{\mathrm{i}n_c y}$. We then expand the velocity and the covariance as a series in μ:

$$\bar{u} = \mu\,\bar{u}_1(y,Y,T) + \mu^2\,\bar{u}_2(y,Y,T) + O(\mu^3)\,, \tag{B1a}$$

$$C = C^e(\boldsymbol{x}_a - \boldsymbol{x}_b) + \mu\,C_1(\boldsymbol{x}_a - \boldsymbol{x}_b, Y_a, Y_b, T) + \mu^2 C_2(\boldsymbol{x}_a - \boldsymbol{x}_b, Y_a, Y_b, T) + O(\mu^3)\,, \tag{B1b}$$

along with the linear and nonlinear operators $\mathscr{L}$ and $\mathscr{N}$ that depend on the fast and on the slow meridional coordinate, y and Y respectively.

We substitute (B1) in (6) and collect terms with equal powers of μ. As discussed in section 4, we further assume that the amplitude A, as well as C_1 and C_2, are independent of the slow coordinate Y. This way operators $\mathscr{L}$ and $\mathscr{N}$ also become independent of Y. In this case, the order μ^0 terms yield the homogeneous equilibrium. Terms of order μ^1 yield the balance:

$$\mathscr{A}\begin{pmatrix}\bar{u}_1\\ C_1\end{pmatrix} \stackrel{\text{def}}{=} \begin{pmatrix}\bar{u}_1 - \mathscr{R}(C_1)\\ \mathscr{L}C_1 - \mathscr{N}(\bar{u}_1, C^e)\end{pmatrix} = 0\,, \tag{B2}$$

which can also be compactly written as

$$\bar{u}_1 = \varepsilon_c f(0|\bar{u}_1, Q/2)\,, \tag{B3}$$

where $f(\sigma|\bar{u}_1, Q/2)$ is the vorticity flux feedback on the mean flow $\bar{u}_1$ as defined in (15). The solution of (B3) is the eigenfunction of operator $\mathscr{A}$ with zero eigenvalue:

$$\begin{pmatrix}\bar{u}_1\\ C_1\end{pmatrix} = A(T)\begin{pmatrix}\mathrm{e}^{\mathrm{i}n_c y}\\ \varepsilon_c\,\mathrm{e}^{\mathrm{i}n_c(y_a+y_b)/2}\left[G_c^+(0|\boldsymbol{x}_a - \boldsymbol{x}_b) - G_c^-(0|\boldsymbol{x}_a - \boldsymbol{x}_b)\right]\end{pmatrix} + \text{c.c.}\,. \tag{B4}$$

In (B6) the subscript c on $G^{\pm}$ denotes that they are evaluated at $n = n_c$. At order μ^2 the balance is:

$$\mathscr{A}\begin{pmatrix}\bar{u}_2\\ C_2\end{pmatrix} = \begin{pmatrix}0\\ \mathscr{N}(\bar{u}_1, C_1) + \varepsilon_c Q\end{pmatrix}\,. \tag{B5}$$

Equation (B5) has a homogeneous solution which is proportional to $[\bar{u}_1, C_1]^T$ and can be incorporated in it, and a particular solution. The nonlinear term $\mathscr{N}(\bar{u}_1, C_1)$ generates both a double and a zero harmonic mean flow (and covariance). As a result, the particular solution is:

$$\begin{pmatrix}\bar{u}_2\\ C_2\end{pmatrix} = \begin{pmatrix}0\\ \varepsilon_c Q(\boldsymbol{x}_a - \boldsymbol{x}_b)/2 + C_{20}(\boldsymbol{x}_a - \boldsymbol{x}_b, T)\end{pmatrix} + \begin{pmatrix}\alpha_2 A(T)^2\,\mathrm{e}^{2\mathrm{i}n_c y}\\ C_{22}(\boldsymbol{x}_a - \boldsymbol{x}_b, T)\,\mathrm{e}^{2\mathrm{i}n_c(y_a+y_b)/2}\end{pmatrix} + \text{c.c.}\,, \tag{B6}$$

where C_{20} and C_{22} are the zero and double harmonic coefficients of the covariance and

$$\alpha_2 \stackrel{\text{def}}{=} \frac{\varepsilon_c \int \frac{\mathrm{d}^2\boldsymbol{k}}{(2\pi)^2} \frac{\mathrm{i}n_c k_x^3 (k^2 - n_c^2)}{2k^2 k_2^2 + 2\mathrm{i}\beta n_c k_x k_{y,1}} \left\{ \frac{k_{y,2}(k_2^2 - n_c^2)}{k^2 k_4^2 + 2\mathrm{i}\beta n_c k_x k_{y,2}} - \frac{k_y k_2^2 (k^2 - n_c^2)}{k^2 (k_{-2}^2 k_2^2 + 2\mathrm{i}\beta n_c k_x k_y)} \right\} \hat{Q}(\boldsymbol{k})}{\varepsilon_c \int \frac{\mathrm{d}^2\boldsymbol{k}}{(2\pi)^2} \frac{2n_c k_x^2 k_{y,2}(k^2 - 4n_c^2)}{k^2(k^2 k_4^2 + 2\mathrm{i}\beta n_c k_x k_{y,2})} \hat{Q}(\boldsymbol{k}) - 1}\,, \tag{B7}$$

with $k_{y,j} \stackrel{\text{def}}{=} k_y + j n_c/2$ and $k_j^2 \stackrel{\text{def}}{=} k_x^2 + k_{y,j}^2$ for any integer j.

At order μ^3 the balance is:

$$\mathscr{A}\begin{pmatrix}\bar{u}_3\\ C_3\end{pmatrix} = \begin{pmatrix}-\partial_T \bar{u}_1\\ -\partial_T C_1 + \mathscr{N}(\bar{u}_2, C_1) + \mathscr{N}(\bar{u}_1, C_2)\end{pmatrix}\,. \tag{B8}$$

If the r.h.s. of (B8) is an eigenvector of operator $\mathscr{A}$ with zero eigenvalue then secular terms appear that produce a mean flow and an associated covariance that are unbounded at $|y|\to\infty$. This occurs when

$$-\partial_T \bar{u}_1 + \mathscr{R}\left\{\mathscr{L}^{-1}\left[-\partial_T C_1 + \mathscr{N}(\bar{u}_2, C_1) + \mathscr{N}(\bar{u}_1, C_2)\right]\right\} \tag{B9}$$

has a non-zero $\mathrm{e}^{\mathrm{i}n_c y}$ component. The secular terms vanish if:

$$\partial_T \bar{u}_1 + \mathscr{R}\left(\mathscr{L}^{-1}\partial_T C_1\right) = f(0\,|\,\bar{u}_1, C^e) + f(0\,|\,\bar{u}_1, C_{20}) + \mathscr{P}_1 f(0|\bar{u}_1, C_{22}\,\mathrm{e}^{2\mathrm{i}n_c(y_a+y_b)/2} + \text{c.c.}) + \mathscr{P}_1 f(0|\bar{u}_2, C_1)\ . \tag{B10}$$

where $\mathscr{P}_j$ is the operator that projects onto the harmonic jn_c (with j integer):

$$\mathscr{P}_j g(y) \overset{\text{def}}{=} \int_\infty g(s)\,\mathrm{e}^{\mathrm{i}jn_c(y-s)}\mathrm{d}s\ . \tag{B11}$$

Equation (B10) determines the equilibration of the most unstable jet. The terms on the r.h.s. of (B10) are nonlinear in $\bar{u}$ and C and they are responsible for the equilibration of the S3T instability. Let us take a closer look into each term in (B10). The second term on the l.h.s. of (B10) is:

$$\mathscr{R}\left(\mathscr{L}^{-1}\partial_T C_1\right) = (\partial_T A)\,(c_1 - 1)\,\mathrm{e}^{\mathrm{i}n_c y}\ , \tag{B12}$$

where

$$c_1 = 1 + \varepsilon_c \int \frac{\mathrm{d}^2\boldsymbol{k}}{(2\pi)^2}\,\frac{n_c k_x^2 k_{y,1} k_2^2 (k^2 - n_c^2)}{(2k^2k_2^2 + 2\mathrm{i}\beta n_c k_x k_{y,1})^2}\,\hat{Q}(\boldsymbol{k})\ . \tag{B13}$$

The first term on the r.h.s. of (B10) is the vorticity flux feedback on $\bar{u}_1$ at criticality

$$f(0|\bar{u}_1, C^e) = A\,\mathrm{e}^{\mathrm{i}n_c y}\ . \tag{B14}$$

The second term on the r.h.s. of (B10) is the vorticity flux feedback between the order μ^1 mean jet $\bar{u}_1$, and the homogeneous order μ^2 eddy covariance C_{20}:

$$f(0|\bar{u}_1, C_{20}) = -c_3^{ec} A|A|^2\,\mathrm{e}^{\mathrm{i}n_c y}\ , \tag{B15}$$

with

$$c_3^{ec} \overset{\text{def}}{=} \varepsilon_c \int \frac{\mathrm{d}^2\boldsymbol{k}}{(2\pi)^2}\,\frac{n_c k_x^4 k_2^2 (k_2^2 - n_c^2)(k^2 - n_c^2)^2}{|2k^2k_2^2 + 2\mathrm{i}\beta n_c k_x k_{y,1}|^2}\left[\frac{2k_{y,1}}{k^2k_2^2 + \mathrm{i}\beta n_c k_x k_{y,1}} - \frac{k_{y,-1}}{k^2k_{-2}^2 + \mathrm{i}\beta n_c k_x k_{y,-1}} - \frac{k_{y,3}}{k_2^2k_4^2 + \mathrm{i}\beta n_c k_x k_{y,3}}\right]\hat{Q}(\boldsymbol{k})\ . \tag{B16}$$

The third term on the r.h.s. of (B10) is the $\mathrm{e}^{\mathrm{i}n_c y}$ component of the vorticity flux feedback between the order μ^1 mean jet $\bar{u}_1$, with wavenumber n_c, and the order μ^2 inhomogeneous eddy covariance C_{22}:

$$\mathscr{P}_1 f(0|\bar{u}_1, C_{22}\,\mathrm{e}^{2\mathrm{i}n_c(y_a+y_b)/2} + \text{c.c.}) = -c_3^{f_{12}} A|A|^2\,\mathrm{e}^{\mathrm{i}n_c y}\ , \tag{B17}$$

with

$$c_3^{f_{12}} \overset{\text{def}}{=} \varepsilon_c \int \frac{\mathrm{d}^2\boldsymbol{k}}{(2\pi)^2}\left\{\frac{n_c k_x^4 k^2 (k^2 - n_c^2)(k_2^2 - n_c^2)}{\left[2k^2k_4^2 + 4\mathrm{i}\beta n_c k_x k_{y,2}\right]\left[2k^2k_2^2 + 2\mathrm{i}\beta n_c k_x k_{y,1}\right]}\left[\frac{k_{y,1}(k_4^2 - n_c^2)}{2k^2k_2^2 + 2\mathrm{i}\beta n_c k_x k_{y,1}} - \frac{k_{y,3}k_4^2(k^2 - n_c^2)}{k^2(2k_2^2k_4^2 + 2\mathrm{i}\beta n_c k_x k_{y,3})}\right]\right.$$
$$\left. + \frac{2n_c k_x^4 k_{y,1} k_2^2 (k_{-2}^2 - n_c^2)(k^2 - n_c^2)^2 (2k_{-2}^2k_2^2 + 2\mathrm{i}\beta n_c k_x k_y)}{(2k^2k_2^2 + 2\mathrm{i}\beta n_c k_x k_{y,1})^2 (2k^2k_{-2}^2 + 2\mathrm{i}\beta n_c k_x k_{y,-1})(2k_{-2}^2k_2^2 + 4\mathrm{i}\beta n_c k_x k_y)}\right\}\hat{Q}(\boldsymbol{k})\ . \tag{B18}$$

The last term on the r.h.s. is the vorticity flux feedback between the order μ^2 mean jet $\bar{u}_2$, with wavenumber $2n_c$, and the order μ^1 eddy covariance C_1:

$$\mathscr{P}_1 f(0|\bar{u}_2, C_1) = -A|A|^2\,\mathrm{e}^{\mathrm{i}n_c y} c_3^{f_{21}}\ , \tag{B19}$$

where

$$c_3^{f_{21}} \overset{\text{def}}{=} \mathrm{i}\,a_2\,\varepsilon_c \int \frac{\mathrm{d}^2\boldsymbol{k}}{(2\pi)^2}\left\{\frac{k^2 - 4n_c^2}{2k^2k_4^2 + 4\mathrm{i}\beta n_c k_x k_{y,2}}\left[\frac{k_{y,1}(k_4^2 - n_c^2)}{2k^2k_2^2 + 2\mathrm{i}\beta n_c k_x k_{y,1}} - \frac{k_{y,3}k_4^2(k^2 - n_c^2)}{k^2(2k_2^2k_4^2 + 2\mathrm{i}\beta n_c k_x k_{y,3})}\right]\right.$$
$$\left. + \frac{k^2 - n_c^2}{k^2(2k^2k_2^2 - 2\mathrm{i}\beta n_c k_x k_{y,1})}\left[\frac{k_{y,-1}(k_2^2 - 4n_c^2)}{2k_{-2}^2 + 2\mathrm{i}\beta n_c k_x k_{y,-1}} - \frac{k_{y,3}k_2^2(k^2 - 4n_c^2)}{2k_2^2k_4^2 + 2\mathrm{i}\beta n_c k_x k_{y,3}}\right]\right\} n_c k_x^3 \hat{Q}(\boldsymbol{k})\ . \tag{B20}$$

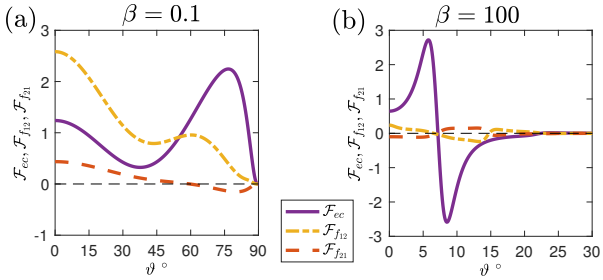

FIG. B10. The contribution of the three feedbacks $\mathscr{F}_{ec}$ (solid), $\mathscr{F}_{f_{12}}$ (dash-dot), and $\mathscr{F}_{f_{21}}$ (dashed) to the nonlinear coefficient $\mathscr{F}_{\rm NL}$. Panel (a) shows the case with $\beta = 0.1$ while panel (b) with $\beta = 100$. The forcing is isotropic ($\gamma = 0$).

Therefore, using (B12), (B14), (B15), (B17), and (B19) we get that (B10) reduces to:

$$c_1\,\partial_T A = A - c_3 A|A|^2\,, \tag{B21}$$

where $c_3 \overset{\text{def}}{=} c_3^{ec} + c_3^{f12} + c_3^{f21}$.

Finally, we arrive to the G–L equation (33) by adding the diffusion term $c_2\partial_Y^2 A$ on the r.h.s. of (B21), with

$$\begin{aligned} c_2 &\overset{\text{def}}{=} -\frac{\varepsilon_c}{2}\left(\frac{\partial^2 f}{\partial n^2}\right)_{n_c,\sigma=0} \\ &= \varepsilon_c \int \frac{\mathrm{d}^2\boldsymbol{k}}{(2\pi)^2}\left[\frac{4k_x^2k_{y,2}^2k^2(k^2-n_c^2)(2k^2+\mathrm{i}\beta k_x)}{(2k^2k_2^2+2\mathrm{i}\beta n_c k_x k_{y,1})^3} - \frac{k_x^2k^2(k^2-4n_c k_y-5n_c^2)}{(2k^2k_2^2+2\mathrm{i}\beta n_c k_x k_{y,1})^2} + \frac{n_c k_x^2 k_{y,1}}{k^2(2k^2k_2^2+2\mathrm{i}\beta n_c k_x k_{y,1})}\right]\hat{Q}(\boldsymbol{k})\,. \end{aligned} \tag{B22}$$

The coefficients c_1, c_2 and c_3 are all functions of β, n_c and the forcing covariance spectrum, $\hat{Q}$. For the ring forcing (4) considered here they are all real and positive.

To study the contribution to each of the components of c_3 from the forced waves with phase lines forming an angle ϑ with the y-axis, we substitute the ring forcing power spectrum (4). After expressing the integrand in polar coordinates $(k_x,k_y) = (k\cos\vartheta, k\sin\vartheta)$ and integrate over k we obtain:

$$[\,c_3^{ec}, c_3^{f12}, c_3^{f21}, c_3\,] = \varepsilon_c \int_0^{\pi/2} \left[\mathscr{F}_{ec}, \mathscr{F}_{f_{12}}, \mathscr{F}_{f_{21}}, \mathscr{F}_{\rm NL}\right] \mathrm{d}\vartheta\,, \tag{B23}$$

where $\mathscr{F}_{ec}$, $\mathscr{F}_{f_{12}}$, $\mathscr{F}_{f_{21}}$ and $\mathscr{F}_{\rm NL}$ is the contribution of the waves with (k_x,k_y), $(-k_x,-k_y)$ and their mirror symmetric $(-k_x,k_y)$ and $(k_x,-k_y)$ to the feedbacks and $\mathscr{F}_{\rm NL} = \mathscr{F}_{ec} + \mathscr{F}_{f_{12}} + \mathscr{F}_{f_{21}}$. Figure B10 shows these contributions as a function of wave angle for isotropic forcing. For $\beta \ll 1$, $\mathscr{F}_{f_{21}}$ is negligible compared to $\mathscr{F}_{ec}$ and $\mathscr{F}_{f_{12}}$. Forced eddies at all angles contribute positively to both $\mathscr{F}_{ec}$ and $\mathscr{F}_{f_{12}}$. The eddies tend to reduce the positive destabilizing contribution $\mathscr{F} > 0$ at small angles mainly through $\mathscr{F}_{f_{12}}$, while they enhance the negative stabilizing contribution $\mathscr{F} < 0$ at large angles mainly through $\mathscr{F}_{ec}$. For $\beta \gg 1$, the dominant contribution comes from $\mathscr{F}_{ec}$ and it follows roughly the same pattern as $\mathscr{F}$. That is, due to the reduction in their energy the eddies tend to reduce both the up-gradient vorticity fluxes of waves with angles $|\vartheta| \lessapprox \vartheta_0$ and the down-gradient fluxes of waves with phase lines at angles $|\vartheta| \gtrapprox \vartheta_0$ with the latter reduction being larger. As a result, the nonlinear feedback of eddies with phase lines at angles $|\vartheta| \gtrapprox \vartheta_0$ is to enhance the jet and, as discussed in section 4, these are the eddies that support the equilibrated jet.

References

Ait-Chaalal, F., T. Schneider, B. Meyer, and J. B. Marston, 2016: Cumulant expansions for atmospheric flows. *New. J. Phys.*, **18 (2)**, 025 019, doi:10.1088/1367-2630/18/2/025019.

Bakas, N. A., N. C. Constantinou, and P. J. Ioannou, 2015: S3T stability of the homogeneous state of barotropic beta-plane turbulence. *J. Atmos. Sci.*, **72 (5)**, 1689–1712, doi:10.1175/JAS-D-14-0213.1.

Bakas, N. A., and P. J. Ioannou, 2011: Structural stability theory of two-dimensional fluid flow under stochastic forcing. *J. Fluid Mech.*, **682**, 332–361, doi:10.1017/jfm.2011.228.

Bakas, N. A., and P. J. Ioannou, 2013a: Emergence of large scale structure in barotropic β-plane turbulence. *Phys. Rev. Lett.*, **110**, 224 501, doi:10.1103/PhysRevLett.110.224501.

Bakas, N. A., and P. J. Ioannou, 2013b: On the mechanism underlying the spontaneous emergence of barotropic zonal jets. *J. Atmos. Sci.*, **70 (7)**, 2251–2271, doi:10.1175/JAS-D-12-0102.1.

Bakas, N. A., and P. J. Ioannou, 2014: A theory for the emergence of coherent structures in beta-plane turbulence. *J. Fluid Mech.*, **740**, 312–341, doi:10.1017/jfm.2013.663.

Bakas, N. A., and P. J. Ioannou, 2015: Emergence of non-zonal coherent structures. *Zonal jets*, B. Galperin, and P. L. Read, Eds., Cambridge University Press, chap. 5, (submitted, arXiv:1501.05280).

Constantinou, N. C., 2015: Formation of large-scale structures by turbulence in rotating planets. Ph.D. thesis, National and Kapodistrian University of Athens, Athens, URL http://www.didaktorika.gr/eadd/handle/10442/35501?locale=en, (also available at arXiv:1503.07644).

Constantinou, N. C., B. F. Farrell, and P. J. Ioannou, 2014a: Emergence and equilibration of jets in beta-plane turbulence: applications of Stochastic Structural Stability Theory. *J. Atmos. Sci.*, **71 (5)**, 1818–1842, doi:10.1175/JAS-D-13-076.1.

Constantinou, N. C., B. F. Farrell, and P. J. Ioannou, 2016: Statistical state dynamics of jet–wave coexistence in barotropic beta-plane turbulence. *J. Atmos. Sci.*, **73 (5)**, 2229–2253, doi:10.1175/JAS-D-15-0288.1.

Constantinou, N. C., A. Lozano-Durán, M.-A. Nikolaidis, B. F. Farrell, P. J. Ioannou, and J. Jiménez, 2014b: Turbulence in the highly restricted dynamics of a closure at second order: comparison with DNS. *J. Phys. Conf. Ser.*, **506**, 012 004, doi:10.1088/1742-6596/506/1/012004.

Cross, M., and H. Greenside, 2009: *Pattern formation and dynamics in nonequilibrium systems*. Cambridge University Press, 552 pp.

Farrell, B. F., and P. J. Ioannou, 2003: Structural stability of turbulent jets. *J. Atmos. Sci.*, **60**, 2101–2118, doi:10.1175/1520-0469(2003)060<2101:SSOTJ>2.0.CO;2.

Farrell, B. F., and P. J. Ioannou, 2007: Structure and spacing of jets in barotropic turbulence. *J. Atmos. Sci.*, **64**, 3652–3665, doi:10.1175/JAS4016.1.

Farrell, B. F., P. J. Ioannou, J. Jiménez, N. C. Constantinou, A. Lozano-Durán, and M.-A. Nikolaidis, 2016: A statistical state dynamics-based study of the structure and mechanism of large-scale motions in plane Poiseuille flow. *J. Fluid Mech.*, **809**, 290–315, doi:10.1017/jfm.2016.661.

Hoyle, R., 2006: *Pattern formation: An introduction to methods*. Cambridge University Press.

Huang, H.-P., and W. A. Robinson, 1998: Two-dimensional turbulence and persistent zonal jets in a global barotropic model. *J. Atmos. Sci.*, **55**, 611–632, doi:10.1175/1520-0469(1998)055<0611:TDTAPZ>2.0.CO;2.

Ingersoll, A. P., 1990: Atmospheric dynamics of the outer planets. *Science*, **248**, 308–315, doi:10.1126/science.248.4953.308.

Ingersoll, A. P., and Coauthors, 2004: Dynamics of Jupiter's atmosphere. *Jupiter: the planet, satellites, and magnetosphere*, F. Bagenal, T. E. Dowling, and W. B. McKinnon, Eds., Cambridge University Press, Cambridge, 105–128.

Marston, J. B., G. P. Chini, and S. M. Tobias, 2016: Generalized quasi-linear approximation: Application to zonal jets. *Phys. Rev. Lett.*, **116 (21)**, 214 501 EP –5, doi:10.1103/PhysRevLett.116.214501.

Monin, A. S., and A. M. Yaglom, 1973: *Statistical Fluid Mechanics: Mechanics of Turbulence*, Vol. 1. The MIT Press.

Parker, J. B., 2014: Zonal flows and turbulence in fluids and plasmas. Ph.D. thesis, Princeton, URL http://arks.princeton.edu/ark:/88435/dsp01h989r543m.

Parker, J. B., and J. A. Krommes, 2013: Zonal flow as pattern formation. *Phys. Plasmas*, **20**, 100 703, doi:10.1063/1.4828717.

Parker, J. B., and J. A. Krommes, 2014: Generation of zonal flows through symmetry breaking of statistical homogeneity. *New J. Phys.*, **16 (3)**, 035 006, doi:10.1088/1367-2630/16/3/035006.

Read, P. L., Y. H. Yamazaki, S. R. Lewis, P. D. Williams, R. Wordsworth, and K. Miki-Yamazaki, 2007: Dynamics of convectively driven banded jets in the laboratory. *J. Atmos. Sci.*, **64**, 4031–4052, doi:10.1175/2007JAS2219.1.

Salyk, C., A. P. Ingersoll, J. Lorre, A. Vasavada, and A. D. Del Genio, 2006: Interaction between eddies and mean flow in Jupiter's atmosphere: Analysis of Cassini imaging data. *Icarus*, **185**, 430–442, doi:10.1016/j.icarus.2006.08.007.

Srinivasan, K., and W. R. Young, 2012: Zonostrophic instability. *J. Atmos. Sci.*, **69 (5)**, 1633–1656, doi:10.1175/JAS-D-11-0200.1.

Srinivasan, K., and W. R. Young, 2014: Reynold stress and eddy diffusivity of β-plane shear flows. *J. Atmos. Sci.*, **71 (6)**, 2169–2185, doi:10.1175/JAS-D-13-0246.1.

Starr, V. P., 1968: *Physics of negative viscosity phenomena*. McGraw Hill, New York, 256 pp.

Thomas, V., B. F. Farrell, P. J. Ioannou, and D. F. Gayme, 2015: A minimal model of self-sustaining turbulence. *Phys. Fluids*, **27**, 105 104, doi:10.1063/1.4931776.

Thomas, V., B. K. Lieu, M. R. Jovanović, B. F. Farrell, P. J. Ioannou, and D. F. Gayme, 2014: Self-sustaining turbulence in a restricted nonlinear model of plane Couette flow. *Phys. Fluids*, **26**, 105 112, doi:10.1063/1.4898159.

Tobias, S. M., and J. B. Marston, 2013: Direct statistical simulation of out-of-equilibrium jets. *Phys. Rev. Lett.*, **110 (10)**, 104 502, doi:10.1103/PhysRevLett.110.104502.

Vasavada, A. R., and A. P. Showman, 2005: Jovian atmospheric dynamics: an update after *Galileo* and *Cassini*. *Rep. Prog. Phys.*, **68**, 1935–1996, doi:10.1088/0034-4885/68/8/R06.